CONDENSED PHASE REACTIONS IN M-2 DOUBLE-BASE PROPELLANTS AT LOW PRESSURES

By

Cecil Eugene Kirby

Submitted in Partial Fulfillment of the

Requirements for the degree of Doctor of Engineering Science

in the Department of Mechanical Engineering

University of South Carolina

1969

College of Engineering
University of South Carolina
Columbia, S. C. 29210

This report is based on the thesis submitted by Mr. C. E. Kirby in partial fulfillment of the requirements for the Degree of Doctor of Philosophy in the College of Engineering, University of South Carolina, Columbia, S. C. The work was supported by Picatinny Arsenal through the Army Research Office - Durham, Grant No. DA-ARO-D-31-124-G1120. The authors are grateful for the support.

N. P. Suh
Project Director

ACKNOWLEDGMENT

The author wishes to acknowledge the guidance, inspiration, and encouragement of Dr. Nam P. Suh, under whose direction this work was performed, and the support given by the National Aeronautics and Space Administration, Langley Research Center, Hampton, Virginia.

TABLE OF CONTENTS

ABSTRACT

An experimental study of the heat of reaction versus pressure for the flameless combustion of M-2 double-base propellant at low pressure has been performed.

Experimental evidence is presented which indicates that the main heat-producing reactions are gas phase reactions which occur very near the surface, and heterogeneous reactions occurring at external surfaces or below the gas-solid interface at surfaces of voids and/or cracks. The overall heat of reaction varies with pressure from approximately 280 cal/gm at 0.3 psia to 560 cal/gm at 75 psia. The apparent activation energies based on scanning calorimeter data are given for this pressure range also. They vary from 47.5 Kcal/mole at 0.3 psia to 60.2 Kcal/mole at 75 psia. Included in these values is the indirectly determined condensed phase heat of reaction of approximately 45 cal/gm for a propellant at an initial temperature of 25° C. This variation of heat of reaction is apparently not continuous but involves jumps in the heat of reaction between 1 and 2 psia, between 14.7 and 25 psia, and another between 110 and 220 psia. This sudden change agrees with other experimental results of the burning rate data obtained at the University of South Carolina, indicating that the reactions near and at the surface dominate the energy generation. The initial stages of reaction from approximately 80° C to 165° C appear to follow a zero-order trend. The onset of significant heating then begins with the initiation of vaporization of nitroglycerine and a change to approximately second-order mode. Orders of reaction were

determined using thermogravimetric analyses. Measurements defining these events were obtained by comparing scanning calorimeter and thermogravimetric data at the same heating rate of 10° C per minute. The effectiveness and response characteristics of these instruments for propellant measurements are also discussed.

Scanning calorimeter results also indicate that nigroglycerine when mixed in with nitrocellulose does not act independently as an ingredient. Low temperature measurements over the temperature range of the freezing point of nitroglycerine of 13° C did not show an endotherm which would be expected if freezing did occur. The fact that nitroglycerine begins to evaporate at approximately 165° C at all pressures confirms this finding.

LIST OF FIGURES

Figure

I. PURPOSE

The purpose of this work is to experimentally investigate reactions occurring in the surface and subsurface regions of M-2 double-base propellants at low pressures (0.3 psia to 75 psia). The work is performed using the techniques of differential scanning calorimetry (DSC) and thermogravimetric analysis (TGA). It is part of an overall program at the University of South Carolina to isolate various critical parameters and determine their effects on the combustion mechanism at low pressures.

II. INTRODUCTION

No reliable combustion model exists for the purpose of burning rate tailoring. Many comprehensive models have been proposed, but they cannot be applied conveniently because of the multitude of parameters that must be numerically known or assumed. The assumptions required are often unverified. A typical analytical treatment involves the independent variation of each parameter to evaluate its effects or to determine the magnitude required to fit experimentally determined burning rate data. More sophisticated analyses only complicate the situation so that application to combustion tailoring has not been analytically possible. There has not been a sufficient number of critical experiments performed on double-base propellants at low pressures to evaluate the importance of various parameters and their effects on the combustion mechanism. Most of the recent literature has dealt with composite propellants or on studies of individual ingredients used in double-base compositions. There is therefore a need to comprehend the deflagration mechanism of double-base propellants at low pressures. Experimental results on the variation of each parameter are not only needed for making improved mathematical models but can provide verification of such models if they satisfy all observed measurements. A model which describes burning rate versus pressure but predicts incorrect surface temperatures and heats of reaction in the various zones would be questionable.

In theoretical treatments of combustion, it has been generally assumed that the burning rate is controlled by gas phase reactions.

Recently, however, Waesche[1] and Wenograd[2] have suggested that condensed phase reactions are the controlling factor in combustion of composite propellants, particularly at low pressures where Wenograd associated the phenomenon of "flameless combustion" with condensed phase reactions. However, the appearance of a visible flame is not a requirement for gas phase reactions to occur. Daniels[3] provided other evidence in support of condensed phase reactions. He examined grains of quenched powder after partial burning and found, by the use of dyes, that there is a changed layer near the surface of the powder which is perhaps 0.015 cm deep.

Rice and Ginell[4] assumed that the powder was appreciably heated to this depth and showed how it could not be accounted for by conduction from the gas phase. However, they did not define what "appreciable" heating was or the effects quenching might have on the surface. Evidence for truly condensed phase subsurface reactions, as opposed to heterogeneous surface coupled reactions with the gas phase is rather flimsy and as this work indicates, at least for M-2 double-base propellants, its significance is very minor.

Some confusion exists in the literature and among workers in the propellants field due to rather loose use of the term "solid phase" reactions. This implies to some people that solid ingredients react and produce solid products. Similarly, the term "condensed phase" implies liquid reactants and liquid product. Most of the literature refers to a decomposition reaction where a solid decomposes to gaseous components as a "solid phase" reaction. These gaseous decomposition products can then react and produce other gaseous products in the

so-called "dark zone" and "flame zone." In the combustion of double-base propellants, it is probable that several different types of reactions occur simultaneously. A better understanding of the phenomena involved may result if these reactions can be defined separately. For the remainder of this thesis, the term "condensed phase" reactions will mean no gaseous products are involved.

One other term which should be clearly defined in any discussion of solid propellant combustion is "surface." It is unlikely that any single plane exists which separates gases from condensed phases. Some condensed phase peaks will protrude into the gas side of the plane, etc. Also in the vicinity of the "burning surface," the temperature gradients are of the order of thousands of degrees per centimeter, and moving a distance of a few microns can change the temperature of a plane of "surface" by significant amounts. Thermocouple beads less than 1 mil in diameter are still large with respect to these gradients; therefore, locating a plane or "surface" by thermocouples is quite difficult. When talking of "surfaces" such as the one on which a minimum surface temperature exists, we must remember that this is a theoretical plane only and may not be relatable to experimental data. This inability to locate a surface naturally confuses the issue of condensed phase heat release if one refers to any reaction occurring in the condensed phase as a condensed phase reaction. The amount of heat released in the condensed phase will naturally vary with the location of the surface. In a high-temperature gradient region where distances of a few microns give significant changes in temperature, the reaction rates which

vary exponentially with temperature can give different answers on the amount of heat released up to a given plane or "surface."

Comparison of DSC and TGA data at the same heating rates shows that no measurable heat is produced before weight loss occurs. Therefore, no condensed phase reactions occur before gas producing reactions start. Decomposition reactions producing gaseous products are most likely to occur at external surfaces; however, some may occur below the gas-solid interface at surfaces of internal voids or cracks in the solid propellant. The visual observance of bubbles at the burning surface of double-base propellants suggests that some gas-producing reactions do occur slightly below the surface. The heat measured by the DSC may be from exothermic decomposition reactions or from gaseous reactions among the decomposition products which occur very close to the surface. Microthermocouple measurements from other work at the University of South Carolina, which will be discussed in detail later, indicate that reactions do occur very close to the surface. Even though condensed phase reactions do not occur before gas-producing exothermic reactions, they still can occur simultaneously with their effects superimposed on the other reactions.

III. LITERATURE REVIEW

Consider the propagation of a one-dimensional combustion wave in a premixed gas as being fixed in space with reactant gases flowing in from the left and product gases flowing out, as shown in figure 1. The steady-state energy equation describing such a flow as given by Frank-Kamenetskii[5] for constant thermal properties is

$$\lambda \frac{d^2T}{dx^2} - \dot{m}C_p \frac{dT}{dx} + W = 0 \qquad (1)$$

where

T = temperature

x = space coordinate

λ = thermal conductivity

$\dot{m}$ = mass flow rate per unit area

C_p = heat capacity of gases

W = volumetric rate of energy release

If we assume the heat release is describable by an Arrhenius expression, then

$$W = \rho Q Z \exp(-E_A/RT) \qquad (2)$$

where R = universal gas constant

Q = energy of reaction in cal/gm

ρ = density

Z = preexponential factor

E_A = activation energy

This premixed gas equation has been solved with the following boundary conditions:

$T = T_o$ at $x = -\infty$ $\qquad$ T_o = initial temperature

$T = T_\infty$ at $x = +\infty$ $\qquad$ T_∞ = flame temperature

The resulting equation, which is given by Pliukhin[6] is

$$\dot{m} = \left[\frac{2\lambda R T_\infty^2 \rho Q Z \exp(-E_A/RT)}{c_p^2 E_A (T_\infty - T_o)^2}\right]^{1/2} \qquad (3)$$

This concept of flame propagation or deflagration accounts for the propagation of flames through gases and is considered by some to be applicable to any continuum.

Combustion of double-base propellants is much more complicated than the combustion of a premixed gas, however, because a solid is involved as well as a gas. Even though the double-base propellant is usually considered to be homogeneous, it may not be truly homogeneous, probably being closer to an emulsion of several compounds because of insolubles in the propellant and the nature of mixing. The decomposition products of this solid may not be in a premixed state. Additional heterogeneous phenomena may also enter. Therefore, many other theories involving the coupling of various zones or phases of solid propellant combustion have arisen.

Heller and Gordon,[7] using high-speed photography, observed that the combustion region of burning double-base propellants consists of three zones. A "foam" zone less than 1 millimeter in depth exists right below the surface in which the solid transforms to a

viscous liquid and bubbles form. Above the burning surface is a large dark zone of supposedly nonreacting gases whose length varies with pressure. As pressure increases, the flame gets closer to the surface. The third zone, which exists only at pressures greater than 100 to 200 psia, depending on the particular propellant, is the flame zone.

In the models of Parr and Crawford[8] and Rice and Ginell[4] shown in figure 2, the "fizz zone" is introduced as an additional one between the "foam zone" and "dark zone" of Heller and Gordon. This "fizz zone" exists even when there is no flame at low pressures. Both of these theories applied the conservation of mass and energy equations to the experimentally observed structure of the combustion zones. They treat each zone consecutively, considering the heat generation in each region and heat feedback from succeeding zones.

Parr and Crawford neglected the "dark zone" and assumed a first-order "foam zone" reaction and a second-order "fizz zone" reaction. The fizz reaction was considered to be the controlling reaction at low pressures where there is no visible flame reaction. They integrated the combined mass and energy conservation equations for the foam and fizz zones, matching the temperatures and extents of reaction at the interface. A temperature T_a was defined to be the temperature at the end of the foam zone when no heat feedback from succeeding zones occurred. A set of tables was provided for ranges of values of activation energy, surface temperature of the fizz zone, and extent of reaction as functions of T_a/T_s. The theory was made to fit burning rate versus pressure curves, hoping that the values of activation

energy, temperature, and extent of reaction thus determined were the correct values. The model predicted a limiting very low pressure coefficient of

$$\pi = \frac{\partial \log m}{\partial \log P} \tag{4}$$

As shown by equation 72 of the cited reference,

$$\pi_{P=0} = 0.50 \tag{5}$$

As the authors themselves point out, the experimental value is 0.75. Therefore, a good fit of the theory cannot be expected at low pressures. It should also be noted that condensed phase reactions (no gases involved) are usually considered to be pressure independent, that is, zero-order reaction. By assuming first-order reactions in the foam zone, Parr and Crawford seem to be implying that the foam zone reaction is heterogeneous.

The approach of Rice and Ginell was quite similar to that of Parr and Crawford except that they neglected the "foam zone" and used empirical data to define the length of the dark zone at various pressures, thereby varying the heat-transfer rate from the flame zone as it moves closer to the surface. The dark zone was considered to be a region in which required concentrations for the flame reaction built up. They included a treatment of the fizz zone when no flame occurred. It also is a curve fitting process in which parameters such as surface temperature with no feedback from the flame and

activation energy for the fizz zone were considered to be the values required to fit the experimental data of burning rate versus pressure.

Adams[9] gives a very interesting treatment of coupling the zones involved in double-base combustion. He includes the diffusion equations for reacting species with the conservation of mass and energy equations. For plane one-dimensional flow, these can be written as

$$M \frac{dG_i}{dx} = -W_i \tag{6}$$

where M is the total mass flux, MG_i is the fractional mass flux for component I, x is the space coordinate, and W_i is the net rate of loss of component I due to chemical change. The diffusion equation is given as

$$MG_i = MY_i - \rho D_i \frac{dY_i}{dx} \tag{7}$$

where ρ is the mass density and Y_i is the mass fraction concentration of component I with mass diffusivity D_i. The energy equation is written as

$$\frac{d}{dx}\left[M \sum G_i h_i - k \frac{dT}{dx}\right] = 0 \tag{8}$$

where h_i, the component enthalpies per unit mass, are defined by

$$h_i = \Delta h_{f_i} + \int^T C_p \, dT \tag{9}$$

and Δh_{f_i} is the standard heat of formation of species I. The summation in equation (8) is taken over all components of the system, and k is defined as the bulk thermal conductivity.

If we assume no heat loss from the combustion products occurs and that the system tends to a state of equilibrium, the derivatives vanish at the hot boundary. The total enthalpy then tends to a constant value and equation (8) can be integrated to give the temperature gradient in terms of the local component mass fluxes and enthalpies as

$$k \frac{dT}{dx} = M \sum G_i h_i - M \sum G_i h_{i \text{ hot boundary}} \qquad (10)$$

If the Lewis number for each species is unity, then $\rho D_i = k/\bar{C}_p$, and if the enthalpy tends to a constant value at the hot boundary, equations (7) and (8) can be combined and integrated to give the result that the local enthalpy remains constant from the cold through to the hot boundary. This can be expressed as

$$\sum Y_i(\Delta h_{f_i} - \Delta h_{f_m}) = \int_T^{T_m} C_p \, dT \qquad (11)$$

where Δh_{f_m} is the standard heat of formation of the final product species, T_m is the temperature at the hot boundary where $Y_m = 1$, and C_p is assumed to be independent of composition. This same result is derived by Rice and Gineil.[4]

Adams then applies these equations to a solid A undergoing an exothermic zero-order reaction to give a gas phase product B which

is then converted to a stable product D in two stages of first and second order, respectively,

$$A \xrightarrow[\text{zero order}]{k_A} B \xrightarrow[\text{first order}]{k_B} C \xrightarrow[\text{second order}]{k_C} D$$

The resulting solution for the mass burning rate is

$$M^2 = \frac{2\bar{k}_a \rho_a Z_a}{C_p(2T_s - T_s' - T_o)} \frac{RT_s^2}{E_a} \exp(-E_A/RT_s) \qquad (12)$$

where

k_a = thermal conductivity of solid phase

ρ_a = density of solid phase

Z_a = frequency factor of solid phase Arrhenius expression

T_s = surface temperature

T_o = initial temperature

T_s' = minimum surface temperature defined by setting the temperature gradient in the gas phase adjacent to the surface equal to zero (no heat feedback from gas phase)

Adams provides plots of the mass fluxes for the solid phase and first-order gas phase reactions as functions of the surface temperature T_s as reproduced below.

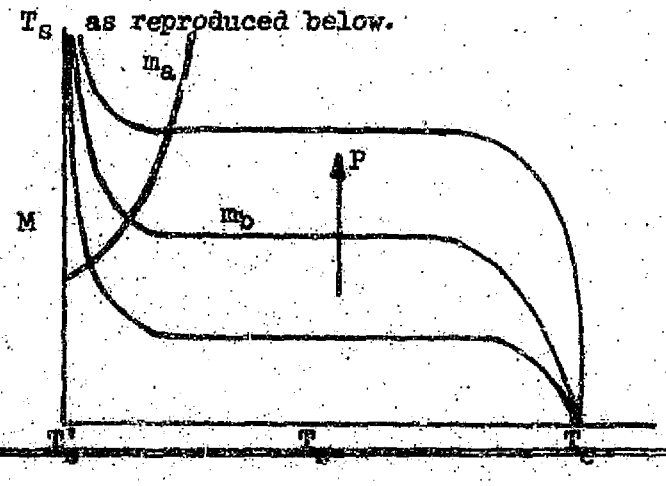

The mass flux for the coupled system and the value of T_s is determined by the intersection of the two curves. The solid phase curve is independent of pressure, but the curves for the first-order gas reaction are shifted vertically upward as the pressure increases, M_b being proportional to the square root of the pressures. Below a certain pressure P^* the intersection lies on the nearly vertical section of the M_b curve where $T_s \rightarrow T_s'$. The burning rate is effectively that of the adiabatic solid phase reaction. Above P^* the intersections occur on the section of the curve which is nearly parallel to the T_s axis. The burning rate is then determined by the gas phase reaction. He also points out that the exact solution of M^2 tends to infinity as $T_s \rightarrow T_s'$.

Even though the above theories have been available since 1950 and experimental measurements to verify their calculated values of activation energy, minimum surface temperature, and heats of reaction in the different zones are clearly needed, they have not been available. One reason may be a general lack of emphasis on double-base propellants in recent years.

For composite propellants, some work has been performed in this area starting about 1966. Waesche[1] and Wenograd[2] have attempted to determine activation energies for condensed phase reactions. These authors assert that the combustion of composite propellants is controlled by condensed phase reactions. The condensed phase reaction is assumed to follow the Arrhenius law and the propellant surface temperature is substituted for the flame temperature in Arrhenius' expression. They assumed zero order kinetics for the solid phase

and assumed that the surface temperature was determined by equilibrium vaporization as suggested by Powling and Smith.[32] Waesche and Wenograd's measurements were taken with a differential scanning calorimeter of the same type used in this work. Using the heat release data from the scanning calorimeter in the mass burning rate equation from the Zeldovitch theory mentioned earlier in this literature review, they obtained fair agreement with predicted deflagration rates in the low-pressure flameless combustion region. Wenograd cited the flameless combustion as evidence for condensed phase reactions. However, as mentioned previously, a visible flame is not a requirement for gas phase reactions to occur. Microthermocouple measurements with double-base propellants at the University of South Carolina by Thompson[10] and scanning calorimeter measurements in this work indicate that gas phase reactions do occur very close to the surface in the case of double-base propellants. Waesche also states that the differential scanning calorimeter is applicable to data acquisition for condensed phase reactions "because the placement of the sensing elements in the base of the sample holders is such that only condensed phase enthalpy changes are measured, and the gaseous reaction products are swept away by the steady purge stream." This statement is true only if there are no gas phase reactions close to the surface of the sample and no heterogeneous attack of the surface by the decomposition products occurs.

Crawford, Huggett, and McBrady[11], using a bomb calorimeter pressurized with nitrogen and using low loading density of propellant, obtained some data on heat of reaction for flameless combustion.

Their data is reproduced in figure 3. The propellant they used is 54 percent nitrocellulose, 43 percent nitroglycerine, and 3 percent ethyl centralyte. It provided flameless combustion below 200 psi. A heat of reaction of 500 cal/gm was reported for flameless combustion. They also analyzed the products of reaction and mentioned that at low pressures (low in their case meaning 20 to 300 psi) an oily residue remained in the combustion chamber. This was thought by them to be glyoxal. Analysis of the products of reaction also suggested to them that nitric oxide and other simple organic molecules react in the gas phase very close to the surface at low pressures. They felt that approximately one-half of the total heat of reaction is liberated in this region and the temperature of the reaction zone rises to perhaps 1,500° K. In the final stages of the reaction, nitric oxide reacts with the remaining oxidizable material and the flame temperature reaches its maximum value of approximately 3,000° K if the pressure is high enough for the flame to exist.

In 1966 a translation of a Russian journal article by Zenin[12] appeared. His experiments were performed in 1958 using thermocouples to determine temperature profiles for deflagration waves. These temperature profiles were used to obtain the amount of heat released in each of the combustion zones and to estimate the heat supply from the gas phase to the condensed phase. The results of Zenin's experiments are shown in figure 4. His results roughly agree with this work even though the methods used in obtaining them are not given in detail and he was not correcting for thermocouple losses and high

temperature gradient effects. Such effects can be significant as shown by Suh and Tsai.[13]

Although the heat of reaction and activation energy as a function of pressure are very important pieces of information, especially at low pressures due to its rapid change, they are not readily available. Lenchitz and Haywood[14] measured the heat of reaction of modified double-base propellants and found it increased with pressure, approaching an asymptotic value. Lenchitz[15] also measured the heat of reaction of M-2 propellant with and without flame and found the difference between the two cases to be small. Using a bomb calorimeter and low loading density, he obtained values of 439 cal/gm, 588 cal/gm, and 783 cal/gm at average burning pressures of 14.7, 111, and 221 psia. Lenchitz's values agree well with the results presented in this work, although the measurement techniques are different.

IV. ARRHENIUS THEORY

Since the Arrhenius expression is used in derlving equations for data reduction in this work and is so widely used in solid propellant combustion literature, it is desirable that it be discussed here. This will give the reader a better appreciation for the limitations of the Arrhenius approach and the assumptions inherent in its use.

Consider a reversible reaction

$$A + B \rightleftarrows C + D \tag{13}$$

Any number of reactants may enter into this reaction and produce any number of products as long as the process is a single-step type and no chain or branch-type reactions are involved. The equilibrium constant K_c of this reaction may be expressed in terms of the forward rate constant k_1 and the backward rate constant k_2 as

$$K_c = \frac{k_1}{k_2} \tag{14}$$

When two reactant molecules have sufficient energy between them and undergo a collision, they enter into a "transition" state which is intermediate between the reactants state and the products state. In the figure below

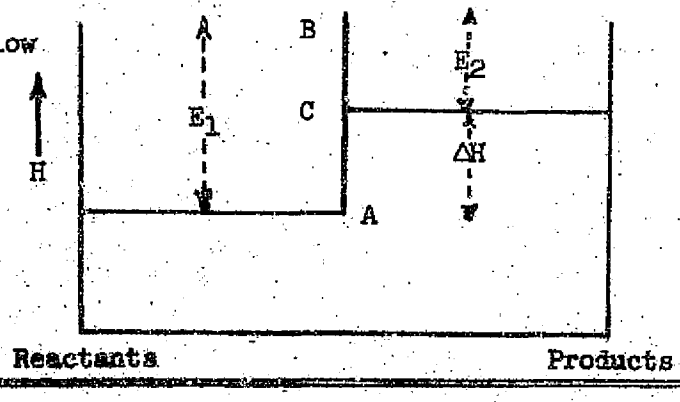

the heat contents (H) of the reactants, products, and transition state are shown diagrammatically. The distance AB corresponds to the difference in energy between the transition state and the reactants state, which equals the activation energy for the forward reaction E_1. The activation energy for the backward reaction E_2 corresponds to distance BC. The heat of reaction ΔH is given by AC. Then we have

$$E_1 - E_2 = \Delta H \tag{15}$$

Using the Van Hoff isochore (see Liepmann and Roshko[33], p. 30) which is

$$\frac{d \ln K}{dT} = \frac{\Delta H}{RT^2} \tag{16}$$

we substitute (14) and (15) in (16) to get

$$\frac{d}{dT}\left(\ln \frac{k_1}{k_2}\right) = \frac{E_1 - E_2}{RT^2} \tag{17}$$

and rearranging this

$$\frac{d \ln k_1}{dT} - \frac{d \ln k_2}{dT} = \frac{E_1}{RT^2} - \frac{E_2}{RT^2} \tag{18}$$

This suggested to Arrhenius that the forward and backward reactions might act independently and he considered the two equations

$$\frac{d \ln k_1}{dT} = \frac{E_1}{RT^2} + C \quad \text{and} \quad \frac{d \ln k_2}{dT} = \frac{E_2}{RT^2} + C$$

where C is a constant. Experiments proved his suggestion to be true, resulting in the simplified form

$$\frac{d \ln k}{dT} = \frac{E}{RT^2} \tag{19}$$

which can be integrated assuming E is independent of temperature to get

$$\ln k = -\frac{E}{RT} + C \tag{20}$$

which can be rewritten as

$$k = A \exp(-E/RT) \tag{21}$$

where A is a constant. This constant is determined by the frequency at which molecules with sufficient energy collide and the orientation requirements for reaction to take place. The exponential portion describes how many molecules can overcome the energy barrier.

In deriving this Arrhenius expression, we are using a grossly simplified case. In reality, reactions are not so simple and the stoichiometric equation illustrated by equation (13) - even if it could be written for the complex mixture of reactants and final products of propellant burning - would not describe the kinetic reactions which actually take place. The real reactions are more likely to be a complex sequence of series, parallel, branching, or chain reactions involving active intermediate species which do not even appear in the stoichiometric equation.

If we use the Arrhenius expression to describe any part of our reactions, we are describing it as an overall reaction with one activation energy. In reality, it is probably a much more complex group of reactions taking place as the experimental results section will show. However, as long as our proposed description agrees with experimental fact, it should be considered useful to the extent that it does express certain overall aspects of the reaction and allows us to predict what might possibly happen under conditions, to some degree, outside of the range of experimental measurements. Since we are not trying to determine the kinetic details of our propellant reactions, but only the overall effects, the approach of assuming an Arrhenius type describing expression does not seem unjustified.

V. EXPERIMENTAL APPARATUS AND PROCEDURE

1. Differential Scanning Calorimeter - (DSC)

A. Description of the Instrument

The scanning calorimeter used in these experiments is manufactured by Perkin-Elmer Corporation. The operators manual[16] describes it as follows: "The operation of the model DSC-1 is based on the temperature control of two miniature sample holders in the sample holder assembly as shown in figure 5. A block diagram of the instrument is shown in figure 6. The system consists of two separate "control loops," one for average temperature control, the second for differential temperature control. In the average temperature loop, a programer provides an electrical signal which is proportional to the desired temperature of the sample and reference holders. The programer temperature information is also relayed to the recorder temperature marker pen and appears as the abscissa scale marking. The programer signal is compared with the average signal from platinum resistance thermometers permanently embedded in the sample and reference holders. The resultant difference signal is amplified in the average temperature amplifier. If the temperature called for by the programer is greater than the average temperature of the sample and reference holders, more power will be fed to the heaters of both sample holders which, like the resistance thermometers, are embedded in the holders. If the average temperature is higher than that demanded by the programer, the power to both heaters will be decreased. In this way, the average temperature of the holders is made to track the command from the programer.

"In the differential temperature control loop, signals representing the sample and reference temperatures, measured by the platinum thermometers, are fed to a circuit which determines whether the reference or sample temperature is greater. The differential temperature amplifier output will then proportion a small increment of power between the reference and sample heaters in such a way as to correct any temperature difference between them. This is done by increasing the power to one while decreasing the power to the other. A signal proportional to the differential power is also transmitted to the main recorder pen. The integral of the resulting peak is the internal energy change. The direction of the pen excursion will depend upon whether more power is required in the sample or reference heater."

The operator raises the average temperature of the sample holders to a desired initial temperature and selects one of eight available temperature program rates between 80° C per minute and 0.625° C per minute. Most of the runs for these experiments were at 10° C per minute or 20° C per minute. When any endothermic or exothermic reaction occurs in the sample, the change in power required to maintain the sample holder at the same programed rate as the reference holder is recorded. The chart abscissa gives the temperature and the area under a curve gives the total energy transfer to or from the sample. The amplitude of the deflection from the baseline represents the exothermic or endothermic heating rate in millicalories per second. The sensitivity to heating rates of various samples is selected from 2, 4, 8, 16, or 32 millicalories per second ranges for full-scale recorder deflection.

Provision is made for removal of decomposition gases by allowing an inert gas to flow into the sample holder assembly. A sketch of the gas flow path is shown in figure 7. Examination of this figure will show how gaseous reactions which occur close to the surface cannot be swept away by the purge gases. The sample holder and its aluminum dome-shaped cover constitute an essentially closed system except for the small amount of purge gas which leaks in around the crack between the holder and cover against the outward flow of decomposition gases. A photograph of the assembled DSC and TGA system is shown in figure 8.

A special low-temperature enclosure to surround the sample holder assembly is provided with the scanning calorimeter for measuring heats of fusion for materials with low temperature melting points. This enclosure is constructed like a wide-mouth vacuum-type "thermos" bottle. Liquid nitrogen can be poured into this enclosure to surround the sides and top of the sample holder assembly with a jacket of liquid nitrogen. The sample holder assembly can thus be cooled to -100° C. Programed scanning rates can be initiated at this temperature. Crushed dry ice and acetone can also be used as a coolant to cool the sample holder assembly to approximately -20° C. The operation of the system is essentially the same with the low-temperature enclosure as with the normal enclosure except that extra liquid nitrogen must be added periodically.

The DSC is calibrated by using a 10 mg lead reference sample. This sample is placed in the sample holder and a programed temperature rise rate of 20° C per minute is initiated. When the melting point of lead (600° K) is reached, the recorder begins moving in the endothermic

direction. If the DSC temperature dial does not read 600° K at the start of this endotherm, the temperature calibration control is adjusted to reduce the difference and the procedure repeated until the dial reads 600° K. The area of the resulting endothermic curve and the known weight and heat of fusion of lead provide a means of calibrating the DSC for accurate measurements of the total heat going into or being generated by a sample. This method automatically accounts for the resistance to heat flow across the interface between the sample holder and the aluminum sample pan which encloses the sample.

B. Modifications for High Pressure Measurements

The DSC-1 scanning calorimeter as available from the manufacturer is capable of measurements at atmospheric pressure and below. For the work reported in this thesis, pressures above atmospheric were desired for comparison with data from other work at the University of South Carolina. An additional sample holder assembly and mounting hardware was obtained from the manufacturer. This extra sample holder was mounted in a spherical pressure vessel shown in the sketch of figure 9 and photographs of figure 10. Electrical connections are tapped into the existing atmospheric system electronics and a switch added to allow use of either sample holder assembly. However, to eliminate possible variations, the high pressure vessel is used for vacuum and high pressure runs. Purge gas and vacuum connections are connected to the pressure vessel also. A continuous purge flow of 20 to 30 cc/min, as measured by flowmeters, is maintained during all runs above and below atmospheric. The pressure

vessel is designed to handle 500 psia safely and was hydrotested to 750 psi before use. However, at pressures above 75 psi, it is difficult to prevent baseline drift. This is probably due to the increase in thermal conductivity of the environmental inert gas which is argon in this case. Argon is used instead of nitrogen because there is some indication that nitrogen affects the reaction processes of double-base propellants. The vacuum, purge gas connections, and valve system for the high pressure DSC system are sketched in figure 11.

C. Sample Preparation and Experimental Procedure

Two different types of samples are used in the scanning calorimeter experiments. The first type is cut from a rod of propellant approximately 1/8 inch in diameter. Disks of 0.025 to 0.030 inch thick are cut, using a lathe and knife-edge cutting tool. Weights range from 16 to 22 milligrams. Each disk is weighed on an analytical balance accurate to 1/10 milligram. Each disk is placed in the small aluminum pans provided with the scanning calorimeter and covered with a lid of aluminum which is pierced to allow gaseous decomposition products to escape. The edges of the pan are then crimped with the special tool provided with the calorimeter to completely enclose the sample disk of propellant. The sample pan is then placed in the sample holder assembly and an empty sample pan placed in the reference sample holder. (This is acceptable in differential scanning calorimetry where the specific heat of the reference material does not have to be similar to the sample as in differential thermal analysis.) The range selection switch is set at either 2 or 4 millicalories per second for full-scale deflection. These are the

most sensitive settings of the instrument. The argon flow control needle valve is then opened enough to allow for a 20 to 30 cc per minute purge flow rate. For runs below atmospheric, the vacuum pump is started and the bypass valve opened to maintain the desired pressure. The argon needle valve is then readjusted for a 20 to 30 cc per minute purge flow rate. For runs above atmospheric pressure, the valve at the entrance to the pressure vessel is opened and the pressure regulator on the argon supply tank is set to the desired pressure. Simultaneous adjustment of the argon needle valve and the outlet valve in the vacuum line provides a purge flow through the same path as for low pressure runs and at the same rate of 20 to 30 cc per minute.

After waiting several minutes for the pressure and purge flow to stabilize, the programer switch is set to 10° C per minute and the start switch turned on to begin the scan. The zero position control is adjusted to position the marking pen in the center of the recorder chart. The slope control is then adjusted to produce a vertical run along the center of the paper when no chemical reactions are occurring. When exothermic reactions start in the sample, the recorder pen deviates from the centerline and moves toward the edge of the paper. When full-scale position is reached, the run is stopped by cutting off the main power switch and argon supply tank valve. Pertinent information is then written on the chart paper for identification of each run. Measurements such as these were made at various pressures between 0.3 psia and 75 psia. Results of these runs are discussed later. This same technique of sample preparation is also used for the low temperature runs. The sample holder assembly is covered with the

liquid nitrogen jacket enclosure and liquid nitrogen added. The temperature of the samples is monitored until equilibrium is reached and then the previous operation procedure is followed. The low temperature runs are performed at atmospheric pressure.

The second method of sample preparation is required to prevent self-heating in runs for which the heat of reaction is measured. If self-heating of the sample due to exothermic reactions exceeds the amount required to maintain the programmed heating rate, inaccurate results are obtained. This is prevented by mixing 10 percent or less of finely powdered propellant with a material known to be chemically inert over the range of temperature and pressure being investigated. Polyphenyl ether,[17] a liquid used as a high temperature hydraulic fluid and as a high vacuum lubricating oil, is a suitable material. It is available from Consolidated Vacuum Corporation[18] under the tradename Convalex-10.

A sample pan of pure polyphenyl ether was scanned over the temperature range of 25° C to 300° C at pressures down to 10 mm Hg and found to be stable and did not vaporize. A known amount of polyphenyl ether is placed on a glass microscope slide and a pre-weighed amount of finely powdered propellant (10 percent or less) is mixed with the polyphenyl ether and stirred to form a slurry. Wrap several turns of No. 30 gage nickel wire around a 20d common nail and cut off one turn of wire to form a ring which will just fit into the aluminum sample pan. A small droplet of slurry is then placed inside of the ring, covered with a lid pierced 10 times with a hypodermic needle and crimped at the edges. The wire ring prevents the liquid from being

squeezed out during the crimping process. The sample pan, ring, and lid are weighed before adding the slurry and afterwards to determine the amount present in each sample pan accurate to 1/10 milligram. Slurry weights of roughly 20 milligrams at 5 to 10 percent propellant produce curves which remain on scale for range settings of 8 to 16 millicalories per second, depending on the pressure. The procedure for setting of pressure and purge flow is the same as for disk samples. For these runs the programed temperature rise rate is allowed to continue until exothermic reactions cease and the marker pen returns to the baseline. The baseline sometimes drifts slightly in the exothermic or endothermic direction, depending on how accurately the slope control is adjusted at the beginning of a run. Several runs at one pressure usually allow a proper setting to be achieved. Some readjustment is usually required when the pressure is changed between runs.

The heat of reaction runs usually produce a bell-shaped curve. The area under the curve bounded by a baseline drawn tangent to the lower edges of the bell is measured with a mechanical planimeter. The planimeter is then used to measure the area of a rectangle which is one-half of the chart in width, and in length equaling 1 minute of run time. (For example, if the chart speed is 4 inches per minute, the rectangle is 4 inches long.) A direct measure of the heat of reaction in calories is then given by

$$\text{Calories} = \frac{(\text{Area of sample peak})(\text{range setting})(60)}{(\text{Area of rectangle})(1000)} \qquad (22)$$

This is then divided by the weight of propellant in the sample to get the heat of reaction in calories per gram.

The procedure given in reference 19 was also tried. The propellant was dissolved in acetone and coated onto an inert solid, cab-o-sil (obtainable from the Cabot Corporation, Boston, Massachusetts). For a known initial amount of cab-o-sil on which a 10 percent solution of propellant in acetone was poured, the weight increase was never 10 percent. Similar mixes produced variable weight changes and nonreproducible heats of reaction. Orders of magnitude of measurements were similar to the polyphenyl ether results, but no definite trends were recognizable.

One other procedure, using small amounts of pure powdered M-2 propellant (less than 2 mg), was tried. The resulting curves will remain on scale for range settings of 32 millicalories per second. These samples also must be enclosed in sample pans with pierced lids to prevent powder fragments from getting out of the sample pan due to purge gas flow or decomposition gas flow and causing spurious peaks on the recorder.

2. Thermogravimetric Analysis System - (TGA)

A. Description of the Instrument

A Perkin-Elmer Model TGS-1 thermogravimetric analysis system is used for weight loss versus temperature measurements. It provides a record of microgram level weight changes in a sample as a function of temperature from ambient to 1,000° C. It utilizes a Cahn "RG" electrobalance which is mounted in a glass vacuum chamber, permitting control of the atmosphere around the sample suspended from the balance beam of the electrobalance into a furnace below it. The Cahn electrobalance provides a sensitivity of 0.0001 mg. The furnace consists of a platinum resistance heating element wrapped around the

outside of a ceramic cylinder 3/8 inch in diameter. The sample is suspended in a sample pan inside the heated ceramic cylinder. The location of the furnace within the chamber permits close coupling of heat source and sample to permit rapid scanning without information loss. The low thermal mass of the furnace allows rapid programed temperature rise rates at 11 selected linear rates from 0.3 to 320° C per minute. The furnace acts as a heater and as a temperature sensor. In the temperature sensing mode, it forms one side of a bridge circuit. The other side of the bridge circuit is driven by the output signal from the temperature programer. An error signal proportional to the temperature error is developed and fed into an amplifier. In the heating mode, the amplifier output is connected to the heater by means of an electronic system which provides 60-cycle power pulses designed to correct the temperature error.

Temperature calibration is accomplished by heating ferromagnetic standards, held in a magnetic field, through their Curie temperatures. The magnetic field is provided by a permanent magnet mounted to a swinging beam which is moved close to the furnace assembly during calibration. The resulting change in magnetic force as the Curie point temperature is scanned appears as a weight loss on the recorder at the corresponding point in the temperature scan. Controls of the TGS-1 are used to adjust the power to the furnace so that the indicated temperatures of the programer approximate the known Curie point temperatures.

The Cahn electrobalance is calibrated by placing known weights in pans suspended from the beam and adjusting the system controls

with and without a sample pan until the balance is properly zeroed. The weight of a sample is determined from the recorder trace and control settings, depending on the selected range of weight change required for full-scale deflection of the recorder. Nominal sample size is 0.5 to 10 milligrams. Mass range settings of 1 milligram to 200 milligrams with a recorder range of 20 micrograms to 20 milligrams full scale are available. Argon is used as the inert environmental gas for the measurements in this work. A photograph of the system is shown in figure 8 and the argon gas system connections are in figure 11.

B. Sample Preparation and Experimental Procedure

Procedures are based on the operators manual[21] provided by the manufacturer. A prime factor in sample preparation is to maintain the best possible thermal contact with the sample pan to give sharp and reproducible results. Sample sizes are used which fall in the optimized range of the instrument of 0.5 to 10 milligrams. The runs at 10° C per minute used a sample of 7 to 8 milligrams. These were cut from the same rods of propellant used for the DSC sample disks. These were cut to a thickness of about 0.010 inch to provide as much surface contact with the sample pan as possible. Aluminum sample pans, approximately the same size as DSC sample pans, were first used but could be used only once. The carbonaceous residue, which remained after a run in which complete deflagration occurs, is difficult to remove without bending or damaging the soft thin pans. The platinum sample pans were found to be more suitable for re-use,

since they could be easily cleaned for re-use by scraping with a small screwdriver point and washing with acetone.

For the low scan rate runs, the thin disk samples of approximately 7 or 8 milligrams are cut down in size by cutting off the edges to make a small square sample of slightly over 1 milligram weight. Using a full-scale deflection setting of 1 milligram with this size sample produces a sigmoid-shaped curve. Several size samples and ranges were tried in order to get the residue weight to remain on scale and utilize the full chart width for good resolution.

The operating procedure is as follows: We assume that the proper tare weights, required for the type pan being used (aluminum or platinum), have been placed on the balance and the preliminary gross balance calibrations made. With the mass dial at 0.0000 and the recorder range dial at 1, zero the recorder using the set 0/10 control. Set the mass dial at 0.5000 and place a 5-milligram precision weight in the sample pan and zero the recorder with the set 5 control. Repeat this process with and without the 5-milligram weight until no change in the zero position occurs (without adjustment of either the 0/10 or set 5 controls). Then with the weight in place, the recorder range set to 1, and the recorder still at zero, rotate the mass dial one full turn clockwise to move the recorder pen to approximate full-scale deflection position. Set the recorder to read exactly full scale with the calibrate recorder control. After this calibration, the value of the weight on the sample pan will be given by the mass dial setting minus the recorder reading to the right of its full-scale position.

A sample of the desired size, as determined by pre-weighing on an analytical balance accurate to 1/10 milligram, is placed in the sample pan. No lid is used on the sample pan as in the DSC. A lid is required in the TGA only when sputtering of the sample may occur, causing some of the sample to fall from the pan. The range is now set so that a 1-milligram weight loss will cause a full-scale recorder deflection. This same range is used for all sample sizes in these experiments and for all scan speeds used. A recorder chart speed proportional to the temperature scan speed which will provide a trace without extremely small or extremely large slopes for ease of data interpretation is selected. The scan rate is selected and the switch turned on to start the heating program. For runs at low heating rates of 0.62 and 1.25° C per minute, a limit control to stop the programed rise rate and automatically cool it back to ambient is available. It is set for a temperature high enough to cover the desired range. This is convenient for long, time-consuming runs, which can be set up and left overnight to be completed automatically. The resulting data is treated in the results and sample calculations sections.

VI. EXPERIMENTAL RESULTS

1. Differential Scanning Calorimeter Results

A. Vaporization of Nitroglycerine from Propellant

In the maximum sensitivity runs using the 20-milligram disk samples, the first recognizable departure from the baseline occurs at approximately 140° C for a heating rate of 10° C per minute. This exothermic indication continues to increase gradually as shown in figure 12. At approximately 165° C, the established trend in the exothermic direction then dips slightly and then resumes its increase. This appears to be an endotherm on top of the established exothermic rate. If the main power switch is cut off prior to 165° C, the propellant sample holder is found to be clean. But, if the temperature is allowed to increase beyond this point, a small amount of brown oily residue is found on the under side of the aluminum dome-shaped cover over the sample holder cup and around the outside of the sample holder cup. This phenomenon consistently occurs at 165° C for all pressures from 0.3 psia to 75 psia at a heating rate of 10° C per minute. At this same temperature and heating rate, TGA results (which will be discussed in detail later) indicate a sudden increase in the rate of weight loss, supporting the idea of vaporization starting at this point. For runs at 5° C per minute the anomaly occurs at 157° C, and at 20° C per minute it occurs at 173° C. This variation with heating rate is a characteristic of reactions with high activation energies (slow reaction rates) which will be discussed in a later section.

To perform an infrared analysis, a sample of this brown oily liquid can be collected by making repeated runs without cleaning

the sample holder assembly. An infrared spectrum of this liquid indicates it is nitroglycerine, as shown by figures 13 and 14. The appearance of this brown oily liquid at low pressures has been noticed by Clary[20] and by Crawford, Hugget, and McBrady.[11] It is thought to be glyoxal by Crawford, Hugget, and McBrady. The infrared spectrum of glyoxal is shown in figure 15. Glyoxal is fluorescent under ultraviolet light. A sample of the brown oily liquid, if exposed to ultraviolet light, does not fluoresce.

After noticing that M-2 propellant with approximately 20 percent nitroglycerine produces this perturbation at 165° C, it would be expected that JPN propellant with 40 percent nitroglycerine would produce a greater effect, and propellant No. 691 with 60 percent nitroglycerine even more. The JPN did not follow a similar path as shown in figure 16, but the No. 691 propellant shows signs of different behavior beginning at about 162° C. It was noticed, however, that the amount of brown oily residue remaining in the sample holder assembly increased with JPN and even more for No. 691. The behavior of a pure nitrocellulose sample is also shown in figure 16. No brown oily residue at all was found in the sample holder assembly after the pure nitrocellulose test.

Since the onset of significant heating begins after this apparent vaporization, it is possible that new reactions are starting. The M-2, JPN, and No. 691 propellants all have different ingredients and different percentages of nitrocellulose and nitroglycerine. The reactions occurring may therefore be different. Some may be

endothermic and some exothermic. They may also be affected by the physical arrangement of these different ingredients in the nitrocellulose-nitroglycerine matrix. A distinct endotherm which would be expected from pure nitroglycerine would not be likely to occur when the molecules are distributed in the propellant and mechanically constrained. The perturbation we are talking about is also quite small and only detectable when using a larger than normal sample at the most sensitive heat detection setting. The behavior of the JPN is probably a more normal behavior. The detection of the very small perturbations of the M-2 and No. 691 propellants was indeed fortunate.

B. Heat of Reaction Versus Pressure

Typical recorder outputs for the heat of reaction runs are shown in figure 17. The heat of reaction varies with pressure as shown in figure 18. Jumps in heat of reaction occur between 14.7 psia and 30 psia, between 1 psia and 2 psia, and again between 110 psia and 220 psia from Lenchitz's data points. The results using pure propellant powder are shown by X's on figure 18. Possible self-heating effects and the difficulty of controlling heat input and distribution in the powder, as opposed to the powder in polyphenyl ether, probably makes the powder results less precise. They are included to show essential agreement with the polyphenyl ether results. This indicates any reaction between the propellant and/or its products of decomposition with the polyphenyl ether, if it exists at all, is very minor. This jump phenomena agrees with the results of Suh and Clary[20], shown in figure 19, and the results of Thompson and Suh.[10] The slopes of the curves in figure 19 are parallel from 2.4 to

14.7 psia with a slope change between 14.7 and 65 psia. From 65 psia to 115 psia, the slopes are again roughly parallel and another change in slope appears between 115 psia and 165 psia. The data of Thompson and Suh indicate that two temperature jumps occur very close to the surface and move toward the surface as pressure increases, as indicated in figure 20. The pressure at which the jumps in temperature touch the surface agree with the jumps in heat of reaction and the change in slope of the burning rate versus initial temperature curves. The plot of burning rate versus pressure on figure 18 indicates the possibility of a jump in the heat of reaction and burning rate at lower pressure. However, this one has not been verified by thermocouple data and is therefore speculative.

The curves of figure 17 are also used to calculate the activation energies as a function of pressure given in table I. The data from the scanning calorimeter is in the form of distances between the heat of reaction curve and a baseline at the associated absolute temperature. This distance is proportional to the rate of heat release from the sample and is therefore proportional to the rate constant. Provided that a plot of the log of distance versus $1/T$ is a straight line, the activation energy can be approximately calculated from the expression derived in the sample calculations section.

$$-E_A = R \frac{\ln d_1 - \ln d_2}{\frac{1}{T_1} - \frac{1}{T_2}} \tag{23}$$

where d_1 and d_2 are distances from the baseline to the heat of reaction curve at temperatures T_1 and T_2. For best accuracy,

values at the extreme ends of the straight line portion are selected to substitute in the above equation. A straight line usually results from points at first detectable deviation up to the point where the rate of rise starts its inflection to go over the top of the bell-shaped curve.

The derivation of this equation does not make allowance for the mass changing. Therefore, in addition to the approximate nature of the Arrhenius expression discussed previously, we have another source of error. A more detailed discussion of the changing mass effect is given in the section on the computer program for DSC simulation of the appendix. This is a basic question which up to now has not been pointed out in the available literature on the application of the DSC to solid propellant decomposition studies. Fortunately, the results of the computer simulation for the DSC heat of reaction curves, including the mass effects, indicate that the results of using this equation are fairly accurate.

C. Nitroglycerine Freezing Point Measurements

A 20-milligram disk prepared as described previously is placed in the freezer compartment of a household refrigerator overnight. This sample is removed and immediately placed in the sample holder assembly. The low temperature enclosure is then placed around the sample holder assembly. A mixture of dry ice and acetone is put in the low temperature enclosure. After holding the temperature of the sample holder assembly at -20° C for approximately 1 hour, a 20° C per minute scan is initiated. A 20° C per minute scan rate allows a

larger temperature range to be covered without adding more dry ice to the low-temperature enclosure and upsetting equilibrium conditions. When the freezing point of nitroglycerine at 13° C is passed, no endothermic changes are seen, even with the calorimeter set for maximum sensitivity. With 20 percent nitroglycerine in a 20-milligram sample, any freezing should have been easily detected. This procedure, when repeated using liquid nitrogen as the coolant and holding the sample at -100° C for 1 hour, produces the same result (i.e., no indication of nitroglycerine freezing).

It is possible that the nitroglycerine molecules influence the nitrocellulose matrix in a manner similar to the way in which lubricants affect some organic plastics. The plastics become soft just as propellants become softer and more pliable as the nitroglycerine content is increased. JPN with nearly 40 percent nitroglycerine is much softer than M-2 propellant with 20 percent. Regardless of the mechanism involved in the softening of nitrocellulose by nitroglycerine, it appears that the nitroglycerine does not exhibit the same properties as a propellant ingredient as it does when it is in pure form.

The liquid nitrogen cooled experiment, if allowed to continue, shows first signs of exothermic reaction beginning between 60° C and 70° C, as shown in figure 21. This agrees with the first signs of weight loss on TGA runs at the same heating rate, and indicates that only surface reactions are involved. If solid phase reactions without gasification existed, heat would be released before weight loss, but this does not occur in any case. The temperature at which

weight loss begins (for the same heating rate) is at least equal to or slightly less than the temperature at which exothermic heat release is detectable. The low temperature runs are used to detect the first signs of heat release. If the normal enclosure for the samples is used, sufficient time is not always available to finish adjustment of the slope control at the maximum sensitivity settings and 10^{o} C per minute rise rate. Starting out at the lower temperature allows plenty of time to establish a straight baseline before reactions occur.

2. Thermogravimetric Analysis System Results

A. Vaporization of Nitroglycerine from Propellant

With an approximately 8-milligram propellant sample at a scan speed of 10^{o} C per minute, the first detectable weight loss begins at approximately 60^{o} C. The weight loss rate increases slightly with temperature as shown in figure 22 up to 165^{o} C where a sudden increase in rate of weight loss occurs. This increase in weight loss rate coincides with the endothermic anomaly from the scanning calorimeter results. This change in slope occurs at the same temperature for different pressures. This is another indication of a possible vaporization beginning, or at least a new type of reaction associated with the vaporization of nitroglycerine. The fact that the temperature at which this occurs does not change with pressure is again an indication that the nitroglycerine does not act independently as an ingredient when it is mixed in the propellant. However, since the particular TGA system can only be used at atmospheric pressure and below, no pressures above atmospheric were investigated.

After the "knee" is reached, the weight loss rate increases very rapidly, and rapid deflagration of the sample results. Cutting off the main power switch after the "knee" does not prevent complete deflagration from occurring as could be done with the scanning calorimeter. Evidently the larger thermal mass of the TGA heating system keeps the temperature up long enough for runaway conditions to occur, whereas the low thermal mass of the scanning calorimeter cools rapidly enough to prevent it.

B. Determination of Order of Reaction

If a small sample of propellant (1 milligram) is placed in the TGA sample pan and exposed to a very slow heating rate of 1.25° C per minute or less, the sample does not reach the runaway condition of deflagration. Instead, a curve shown in figure 23 results. A solid carbonaceous residue of approximately 10 to 15 percent of the original weight remains. It is believed that this carbonaceous material could also be a product in the flame zone of a burning propellant, since glowing carbon particles are what cause the flame to be visible. Using the method of Kuang-Hua[23], a plot of

$$\frac{\Delta \ln \frac{dW}{dt}}{\Delta \ln W_r} \text{ versus } \frac{\Delta \frac{1}{T}}{\Delta W_r}$$

produces a straight line and the order of reaction is given by the intercept on the $\frac{\Delta \ln \frac{dW}{dt}}{\Delta \ln W_r}$ axis.

The derivation of this equation is reproduced in the sample calculations section. The order of reaction appears to follow an

apparent zero-order trend up to 160° C where it then changes to approximately second order as shown by Figure 24. This curve is based on slide rule calculations. In order to achieve more accuracy, since some of the mass ratios involved are very close to 1 in value and close together, a computer curve fitting method is used. A description of this program and the Fortran statements are included in the sample calculations section.

The computer results indicate a zero-order reaction up to the "knee" of the curve at approximately 150° C and then a change to approximately a second-order reaction. Portions of the computer printout sheets for this curve are shown in figures 25 and 26. Figure 25 is in the vicinity of the "knee" of the curve, which occurs at a weight value of approximately 0.984 milligram in figure 23. Values in column 1 are the assumed orders of reaction which the computer is told to examine for best fit to the experimental curve. Columns 2 and 3 are the weights at the ends of the interval under consideration. Column 4 is the activation energy which makes the assumed order fit the experimental data best. Column 5 is the pre-exponential factor for the best fit. Columns 6 and 7 are the actual error and a root mean square absolute value error. Column 6 is the one the computer uses to select the best overall fit which is given in the last row for a given interval (after the highest assumed order row). An overall best fit is not always calculated because of the characteristics of the program, unless column 6 shows a positive and negative value within the range of assumed orders. Notice that no best fit value is found for the interval 1.034 to 0.984 or for

intervals prior to that, but the least error is at zero order and decreasing. Over the next interval, the order goes to 1.687 and increases thereafter. The average value of the order for the next 10 intervals is 2.162 and the average activation energy over this interval is 43,900 cal/mole. At the end of these 10 intervals, the weight of the sample is down to 0.434 milligram and the temperature is approximately 180° C. The intervals are equally spaced, based on 0.050 milligram weight loss per interval. The change of order at the "knee" of the curve is not unexpected, based on the premise of nitroglycerine vaporization beginning at this point as with the other TGA and DSC curves. The occurrence of this "knee" near 150° C as opposed to the "knee" in figure 20 at 165° C is due to the lower heating rate of 1.25° C per minute.

The same computer procedure was attempted on the samples which reached runaway deflagration conditions at the higher heating rates. Due to the rapid changes of weight loss after the "knee" of such curves, good inputs for the computer, which works over small intervals, are hard to obtain from the curves. However, based on the trend of error decrease, the order was nearer zero before the "knee" and changed to higher order after it.

3. Condensed Phase Heat of Reaction

The original intent of this investigation was to determine the effects of pressure on condensed phase reactions. The use of the differential scanning calorimeter, which has been used by others to obtain such information, is apparently inadequate, at least for double-base propellants. The question then arises as to how one can obtain

the condensed phase heat of reaction or heat of decomposition. This can be obtained by the following interpretation of autoignition measurements made at the University of South Carolina as described by Suh, Tsai, Thompson, and Moore.(24)

Cylindrical rods of M-2 propellant like the ones used to make the disk samples described in the experimental procedures section of this paper were coated with Epon Adhesive 946 (0.003 cm thick) for planar burning. The coated propellant was cut into 2.75-inch lengths. Into each length two No. 80 size holes for indium burn wires and one No. 75 size hole for the thermocouple were drilled. The propellant was then placed in a stainless steel test chamber and connections made, as shown in figure 27. The indium wire used was Indalloy Intermediate Solder No. 6, 30 gage, with melting point of 280 to 285° C. The thermocouple was made of 30 gage, single stranded, enameled iron and constantan wires joined together by resistance welding.

After having completed the above steps, the propellant temperature was raised slowly to some desired value by passing heated air around it, and the temperature history was recorded. Once the propellant temperature reached the desired level, it was ignited by a hot wire heater made of platinum wire. As the flame front passed through the sections containing the indium wires, they melted, yielding the information needed to calculate the burning rate. The above procedure was used with air as the surrounding atmosphere for the propellant. For the series of tests done with argon as the surrounding atmosphere, 2 minutes before igniting the propellant the air supply was turned off and the argon supply was turned on.

Figure 28 shows the experimental results for burning rate as a function of initial temperature. The experimental results obtained using both argon and air fall on the same line. The asymptotic temperature at which the burning rate approaches infinity is found to be 145° C (290° F). This is defined to be the autoignition temperature.

This experiment provides us with a very useful piece of information, which is the minimum surface temperature at the solid surface with no heat feedback from the gas phase. The experimental arrangement indicates that if a piece of propellant is heated to 145° C, it is just about to ignite by itself and the slightest amount of energy which is added to it externally results in sudden ignition and very rapid deflagration at a rate approaching infinity. Theoretically, a burning surface temperature of 146° C would be sufficient to insure burning of a propellant preheated to 145° C at a rate approaching infinity. This experimentally determined value can be used in the theory of Adams[9] to obtain the pure condensed phase heat of reaction. Here we rewrite, for convenience, Adams' equation from the literature review section, that is,

$$\sum Y_i(\Delta h_{f_i} - \Delta h_{f_m}) = \int_T^{T_m} C_p \, dT \qquad (11)$$

Normally, Δh_{f_m} is the standard heat of formation of the final product species, and T_m is the flame temperature at the hot boundary. If Δh_{f_i} represents the heat of formation of reactant species, the left side of this equation is the definition of heat of reaction. Since at the hot boundary $Y_m = 1$ we can take an average value of C_p,

considered as a constant, and $C_p(T_m - T)$ gives us the overall heat of reaction for the propellant burning. However, if we are interested in the condensed phase heat of reaction only, we now have a value for which the temperature gradient at the solid surface is zero, corresponding to the temperature gradient of zero at the hot boundary in the above expression. This value is the minimum surface temperature value obtained by the autoignition measurements. Equation (11) can be applied to the condensed phase region considering Δh_{f_m} as the heat of formation of condensed phase products and Δh_{f_i} as the reactant species again. Now our hot boundary temperature is 145° C and $C_p(145 - T)$ gives us the heat of reaction for the condensed phase reaction (i.e., no gaseous products formed).

If we wish to determine the heat of decomposition for the reaction which produces gaseous decomposition products, we would have to determine the temperature of the gases which result from the decomposition before these products react to form the final gaseous product species. If this temperature were known (without any heat feedback from gaseous product reactions), we could follow a similar procedure as before to determine the heat of decomposition for the reaction producing gases from the solid propellant. As yet this value is not available.

The condensed phase heat of reaction for M-2 propellant at an initial temperature of 25° C is therefore given by

$$H_c = 0.37(145 - 25) = 45 \text{ cal/gm} \qquad (24)$$

It is thus a simple matter to determine the condensed phase heat of reaction for any propellant for which the autoignition temperature and specific heat can be obtained.

Adams' theoretical equation for the mass burning rate discussed in the literature review section, that is,

$$M^2 = \frac{2k_a\rho_a Z_a}{C_p(2T_s - T_s' - T_o)} \frac{RT_s^2}{E_a} \exp\left(-\frac{E_a}{RT_s}\right) \qquad (12)$$

also indicates that if M-2 propellant is preheated to the minimum surface temperature, then $T_s = T_o = T_s' = 145^\circ$ C, and the denominator of equation (12) goes to zero and an infinite burning rate results

Equation (3.6) of Pliukhin[6] which is

$$M^2 = \frac{2kRT_s^2 W_s}{E_s(C_pT_s - C_pT_o)^2} + \frac{k^2\left(\frac{dT_s}{dx}\right)^2}{(C_pT_s - C_pT_o)^2} \qquad (25)$$

also implies this type behavior. Since dT_s/dx equals zero at the surface under no heat feedback conditions, the second term equals zero. If $T_o = T_s$ in the denominator of the first term, the mass burning rate again goes to infinity.

This value of approximately 45 cal/gm agrees in order of magnitude with Zenin's[12] value of 80 cal/gm. The composition of his propellant is not given and his results are based on thermocouple data uncorrected for lead losses. Zenin's method of obtaining the heat release below the surface from thermocouple data would include heat generation from pure condensed phase reactions and from any heterogeneous or gas phase reactions occurring at voids or other surfaces

below the solid gas interface. This would naturally be expected to give a higher value. Zenin also indicates that if the pressure is lowered enough (0.5 mm Hg) gas effects are negligible. If the line of pressure versus heat of reaction in figure 18 is extrapolated to 0.5 mm Hg, a value between 50 and 100 calories per gram is obtained. This is given as a matter of interest only, because extrapolation over three orders of magnitude is rather dubious.

VII. COMPUTER SIMULATION OF DSC

As discussed previously in the DSC results section, there is a time dependence associated with the sample under test for different heating rates. The apparent endothermic anomaly relating to the vaporization of nitroglycerine which occurs at 165° C with a heating rate of 10° C per minute shifts to 157° C for a heating rate of 5° C per minute and to 173° C for a heating rate of 20° C per minute. The bell-shaped heat of reaction curves also shifted at different heating rates, as shown in figure 30.

In order to determine if this is due to the time dependence of the sample rather than a characteristic of the DSC, an equation was written describing the heat release rate as a function of time including mass change effects. This equation, for which the derivation and method of solution are given in the sample calculations section of the appendix, is

$$Q = \int_0^{\tau} \frac{m_o}{1 + T^2 \frac{AR}{ET_o}} \exp\left(-\frac{E_d}{RT}\right) H_{rf} \exp\left(-\frac{E}{RT}\right) d\tau \qquad (26)$$

The digital computer results for the solution of this equation are given in figure 31. The changes in the locations of the peaks and the shapes of these curves approximately agree with the experimentally determined curves of figure 30.

The DSC value for activation energy of 51,500 cal/mole and frequency factor of 10^{21} did not produce the desired curves. It was necessary to reduce the activation energy to 45,000 cal/mole and the frequency factor to 10^{20} in order to get the curve to return close to

zero on the high temperature side of the bell shape. The corresponding values for the mass loss expression which produced the desired curve shapes were $E_a = 56,000$ cal/mole and $A = 10^{24}$ which roughly agree with the experimental values as shown in figure 26.

The fact that the independently obtained DSC and TGA experimental values agree this well and could be used together to reproduce the heat of reaction curve shapes provides some assurance of their accuracy. The use of the Arrhenius expression and equation (A-5) seems justified, and the shift of the peaks is due to the propellant and not the DSC.

This procedure provides a method of checking activation energies which accounts for mass loss effects and is probably more accurate than present methods.

VIII. CONCLUSIONS

Experimental measurements of the overall heat of reaction for M-2 double-base propellants at low pressures are presented for the first time. Agreement with independently obtained results of burning rate and thermocouple data of others indicates the values are reasonably accurate.

The differential scanning calorimeter, when used independently, cannot measure condensed phase heat generation in double-base propellants because of gas phase reactions which occur close to the burning surface. It can be used in conjunction with thermogravimetric analysis measurements (taken at the same heating rate) and high response microthermocouple measurements near the burning surface. Comparison of data from these three sources indicates that the main heat producing reactions in M-2 double-base propellants are gas phase reactions occurring near the surface and heterogeneous surface reactions which may occur at external surfaces or at surfaces of voids and cracks below the burning surface.

Vaporization of nitroglycerine from the propellant has been verified. The beginning of vaporization coincides with the beginning of significant heat release and weight loss rate. The probable order of reaction is zero up to the point where vaporization begins and then a change to approximately second order occurs.

An indirect method of determining the condensed phase heat of reaction is given. It is based on the determination of an artificially defined minimum surface temperature using autoignition measurements.

IX. RECOMMENDATIONS

The next area of investigation should be directed toward measuring the amount of gas-producing reactions occurring below the gas-solid interface and possibly separating this from the condensed phase contribution. This has already been initiated at the University of South Carolina.

A very low pressure chamber for use with the differential scanning calorimeter could be constructed to measure the heat produced at pressures of 0.5 mm Hg and below. If gas phase reactions can be eliminated at such pressures as claimed by Aleksandrov[31], the heat of reaction may reach a constant value. However, it could be just the reactions among gaseous decomposition products which would cease at these pressures. Decomposition reactions may still occur and produce gaseous products which do not react further. If a TGA chamber for these low pressures could also be constructed, weight loss measurements in conjunction with the DSC measurements at very low pressures may determine if this is occurring. The true condensed phase heat of reaction can only be obtained if heat changes can be measured while no gases are being produced, that is, no weight loss occurring as determined by TGA measurements at the same pressure and heating rate.

High pressure TGA measurements should also be performed. The jumps in burning rate shown on figure 17 should be indicated by a change in weight loss rate in this pressure range.

Individual ingredients used in the composition of double-base propellants do not act in the mix as they do independently. Therefore,

in future studies less emphasis should be placed on individual ingredient studies and more on the mixture.

An overall program similar to the one which has been performed on double-base propellants at the University of South Carolina should be repeated for composite propellants. This should include combined DSC, TGA, and high response microthermocouple measurements as well as autoignition and burning rate versus initial temperature measurements.

REFERENCES

1. Waesche, R. H. W.: "Research Investigation of the Decomposition of Composite Solid Propellants," United Aircraft Research Laboratories Report F910476-12, Sept. 1967.

2. Wenograd, J.: "Study of the Kinetics and Energetics of Propellant Decomposition Reactions and Application to Steady State Combustion Mechanism," CPIA Publication No. 138, vol. 1, 89-98, Feb. 1967.

3. Wilfong, R. E.; Penner, S. S.; and Daniels, F.: "An Hypothesis for Propellant Burning," J. Phys. and Coll. Chem. 54, 863-872, 1950.

4. Rice, O. K.; and Ginell, R.: "The Theory of the Burning of Double-Base Rocket Powders," J. Phys. and Coll. Chem. 54, 885-916, 1950.

5. Frank-Kamenetskii, D. A.: Diffusion and Heat Exchange in Chemical Kinetics, Princeton Univ. Press, 1955.

6. Pliukhin, B. I.: "On the Stationary Theory for Heat Balance of Powder and Explosive Condensed Phases," Eighth Symposium on Combustion, 734-745, 1961.

7. Heller, C. A.; and Gordon, A. S.: "Structure of the Gas Phase Combustion Region of a Solid Double-Base Propellant," J. Phys. and Coll. Chem. 59, 773-777, 1955.

8. Parr, R. G.; and Crawford, B. L.: "A Physical Theory of Burning of Double-Base Rocket Propellants," J. Phys. and Coll. Chem. 54, 929-955, 1950.

9. Adams, G. K.: "The Chemistry of Solid Propellant Combustion: Nitrate Ester or Double-Base Systems," Proceedings of the Fourth Symposium on Naval Structural Mechanics, 117-146, Purdue University, Lafayette, Indiana, April 19-21, 1965.

10. Thompson, C. L., Jr.; and Suh, N. P.: "A Theoretical Model for Deflagration of Double-Base Propellants" to be submitted at AIAA Eighth Aerospace Sciences Meeting, New York, N.Y., Jan. 1970.

11. Crawford, B. L., Jr.; Huggett, C.; and McBrady, J. J.: "The Mechanism of the Burning of Double-Base Propellants," J. Phys. and Coll. Chem. 54, 854-862, 1950.

12. Zenin, A. A.: "Burning of Nitroglycerine Powder in Vacuum and at Subatmospheric Pressures," Fizika Goreniya i Vzryva. 2, 74-78, 1966.

13. Suh, N. P.; and Tsai, C. L.: "Thermocouple Response Characteristics in Deflagrating Low Conductivity Materials," submitted to J. Heat. Transfer.

14. Lenchitz, C.; and Haywood, B.: "Determination of the Ballistic Modifier in Propellant Combustion Using the Heat of Explosion Test," Combustion and Flame, 10, 140-146, 1966.

15. Lenchitz, C.: Private communication.

16. Instructions, Differential Scanning Calorimeter, Perkin-Elmer Corporation, No. 990-9509, Sept. 1965.

17. Wilson, D. R.; Marshall, W. A.; Dolle, R. E.; and Benzing, R. J.: "Physical Chemical and Mechanical Characteristics of a Polyphenyl Ether," Ind. and Eng. Chem. 6, 81-88, June 1967.

18. High Vacuum Equipment Data Bulletin 11-6, Consolidated Vacuum Corporation, Rochester, N.Y., 1968.

19. Musso, R. C.; Grigor, A. F.; and Miller, R. R.: "Combustion Mechanism of Low Burning Rate Propellant," Sixth Progress Rept. Contract No. F04611-C-67-0049, Hercules, Inc., Alleghany Ballistics Laboratory, Cumberland, Md., July 1968.

20. Clary, D. L.: The Steady State Burning Rate of Double-Base Solid Propellants at Low Pressures and Various Initial Temperatures, M.S. Thesis, University of South Carolina, 1968.

21. Instructions, TGS-1 Thermobalance, Perkin-Elmer Corporation. No. 990-9398, May 1968.

22. Sammons, G. D.: "Application of Differential Scanning Calorimetry to the Study of Solid Propellant Decomposition," Third ICRPG Combustion Conference CPIA Publication 138, 75-83, Feb. 1967.

23. Kuang-Hua, H.: Application of Thermogravimetric Method and Differential Thermal Analysis in the Study of Reaction Kinetics. Picatinny Arsenal Publication, Dover, N.J., 1967.

24. Suh, N. P.; Tsai, C. L.; Thompson, C. L.; and Moore, J. S.: "The Ignition and Surface Temperatures of Double-Base Propellant at Low Pressure I - Thermocouple Measurements."

25. Boys, S. F.; and Corner, J.: "The Structure of the Reaction Zone in a Flame," Proc. Roy. Soc., A197, 90, 1949.

26. Hastings, C., Jr.: Approximations for Digital Computers," Rand Corporation, 1700 Main St., Santa Monica, Calif., Nov. 1954.

27. Nelson, J. B.: "Determination of Kinetic Parameters of Six Ablation Polymers by Thermogravimetric Analysis," NASA Technical Note D-3919, Langley Research Center, April 1967.

28. Farmer, R. W.: "Thermogravimetry of Plastics Part I - Empirical Homogeneous Kinetics," Tech. Documentary Rept. ASD-TDR-62-1043, Wright-Patterson AFB, Ohio, Feb. 1963.

29. O'Neill, M. J.: "The Analysis of a Temperature-Controlled Scanning Calorimeter," Analytical Chemistry, 36, 1238-1245, June 1964.

30. Watson, E. S.; O'Neill, M. J.; Justin, J.; and Brenner, N.: "A Differential Scanning Calorimeter for Quantitative Differential Thermal Analysis," Analytical Chemistry, 36, 1233-1238, June 1964.

31. Aleksandorv, V. V.; Konev, E. V.; Mikeev, V. F.; and Khlevnoi, S. C.: "Surface Temperature of Burning Nitroglycerine Powder," Fizika Goreniya i Vzryva, 2, 68-73, 1966.

32. Powling, J.; and Smith, W. A. W.: "The Surface Temperature of Burning Ammonium Perchlorate," 10th Symposium on Combustion, 1373-1380, Pittsburgh, 1965.

33. Liepmann, H. W.; and Roshko, A.: Elements of Gas Dynamics, GALCIT Aeronautic Series, John Wiley and Sons, Inc., New York, 29-30, 1960.

34. Pristera, F.; Halik, M.; Castelli, A.; and Fredricks, W.: "Analysis of Explosives Using Infrared Spectroscopy," Analytical Chemistry, 32, 495-508, April 1960.

35. Harris, R. K.: "Vibrational Assignments for Glyoxal, Acrolein, and Butadiene," Spectrochimica Acta, 20, 1129-1141, 1964.

TABLE I.- VARIATION OF ACTIVATION ENERGY WITH PRESSURE

Pressure	Average E_a Kcal/mole	Values used to average
75 psia	60.2	59.0, 65.2, 56.3
50 psia	57.6	56.0, 61.3, 56.1, 57.0
25 psia	55.0	55.0, 56.3, 54.6, 54.0
14.7 psia	51.5	52.0, 50.5, 51.6, 52.8
200 mm Hg	51.4	50.0, 53.2, 51.0
100 mm Hg	48.8	49.8, 47.8, 49.0
50 mm Hg	48.1	47.0, 48.4, 48.8
20 mm Hg	47.7	47.5, 47.8

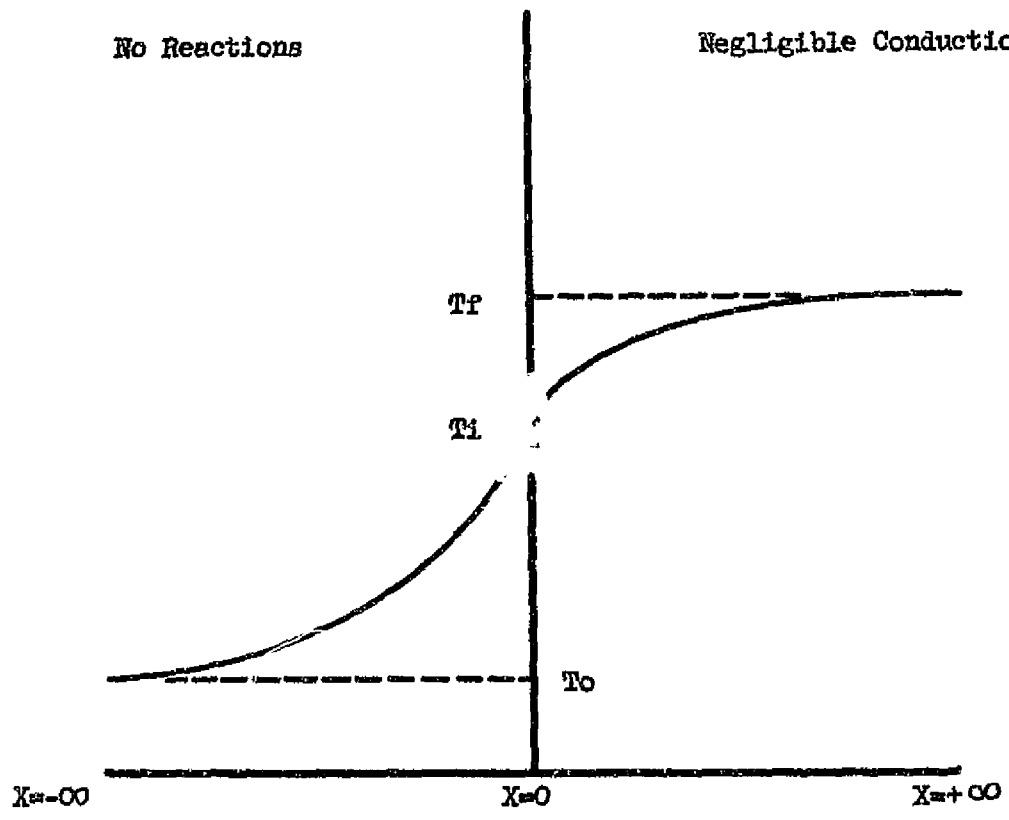

Figure 1.- Zeldovitch premixed gas model.

(a)

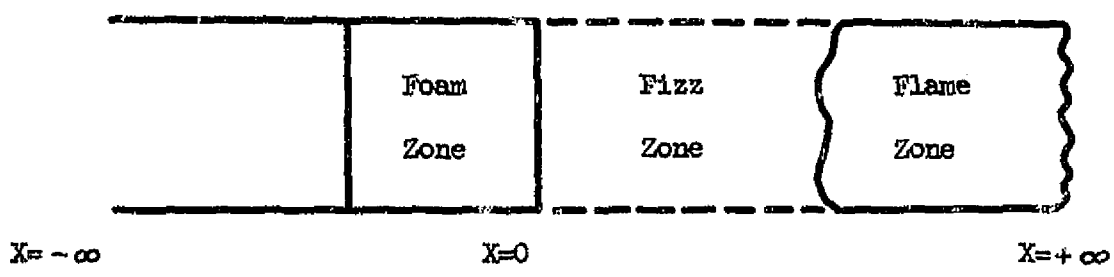

(b)

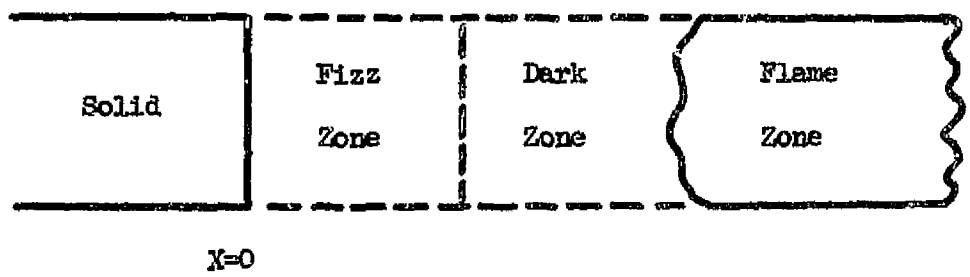

Figure 2.- Models of Parr and Crawford (a) and Rice and Ginell (b).

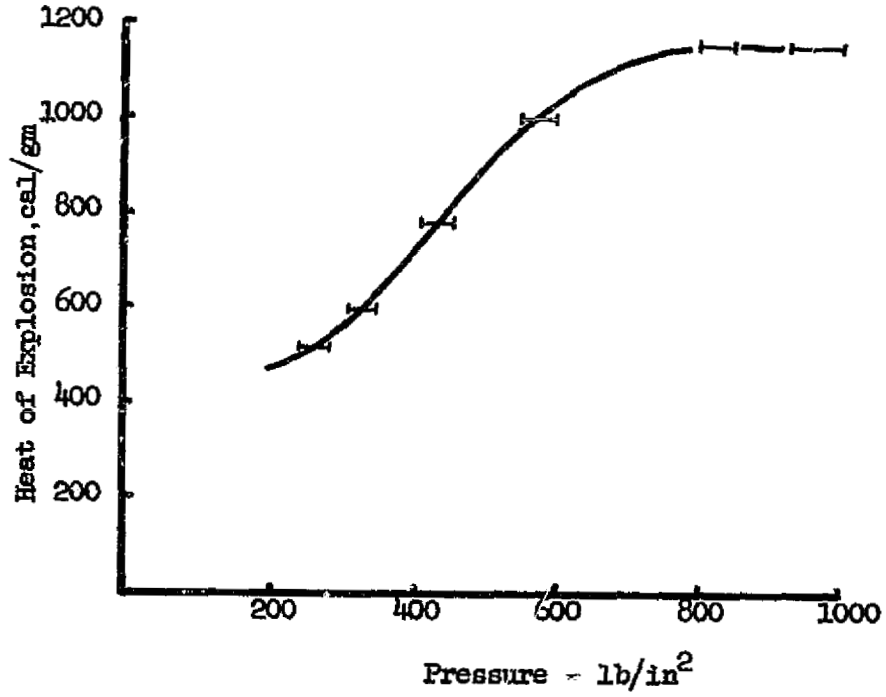

Figure 3.- Heat of explosion versus pressure from Reference 11.

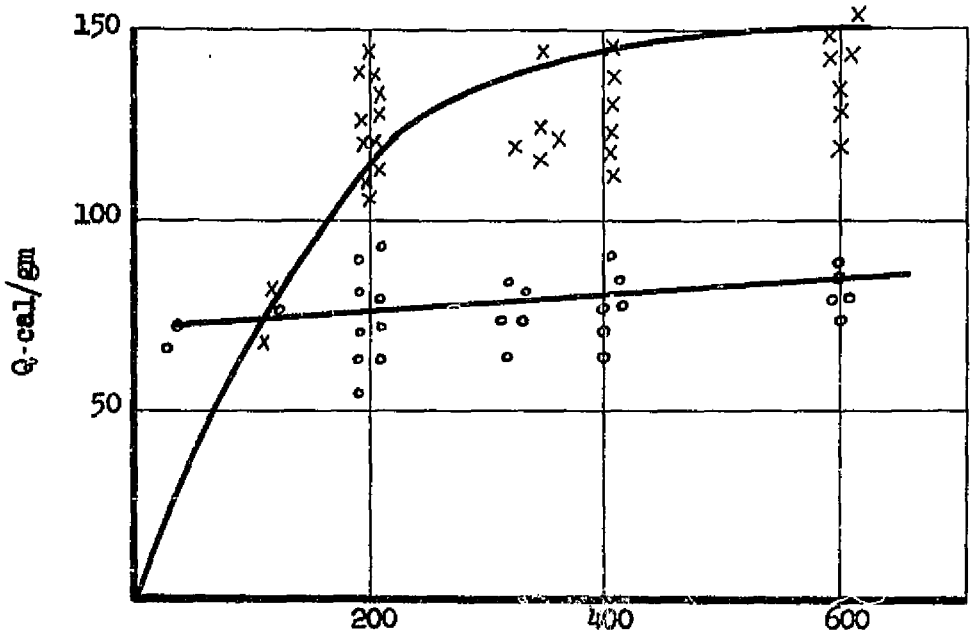

Figure 4.- Heat release per gm of propellant (Ref. 12).

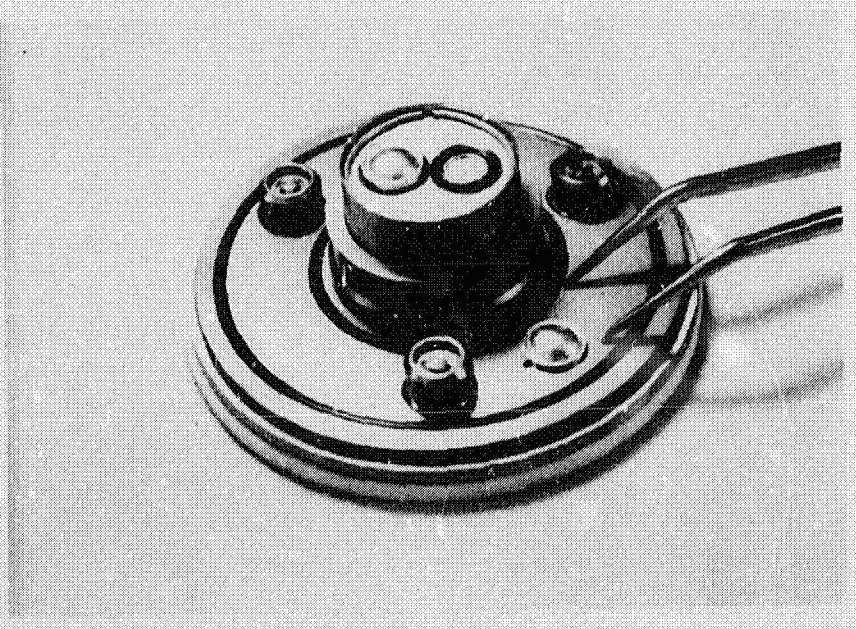

Figure 5.- DSC sample holder assembly.

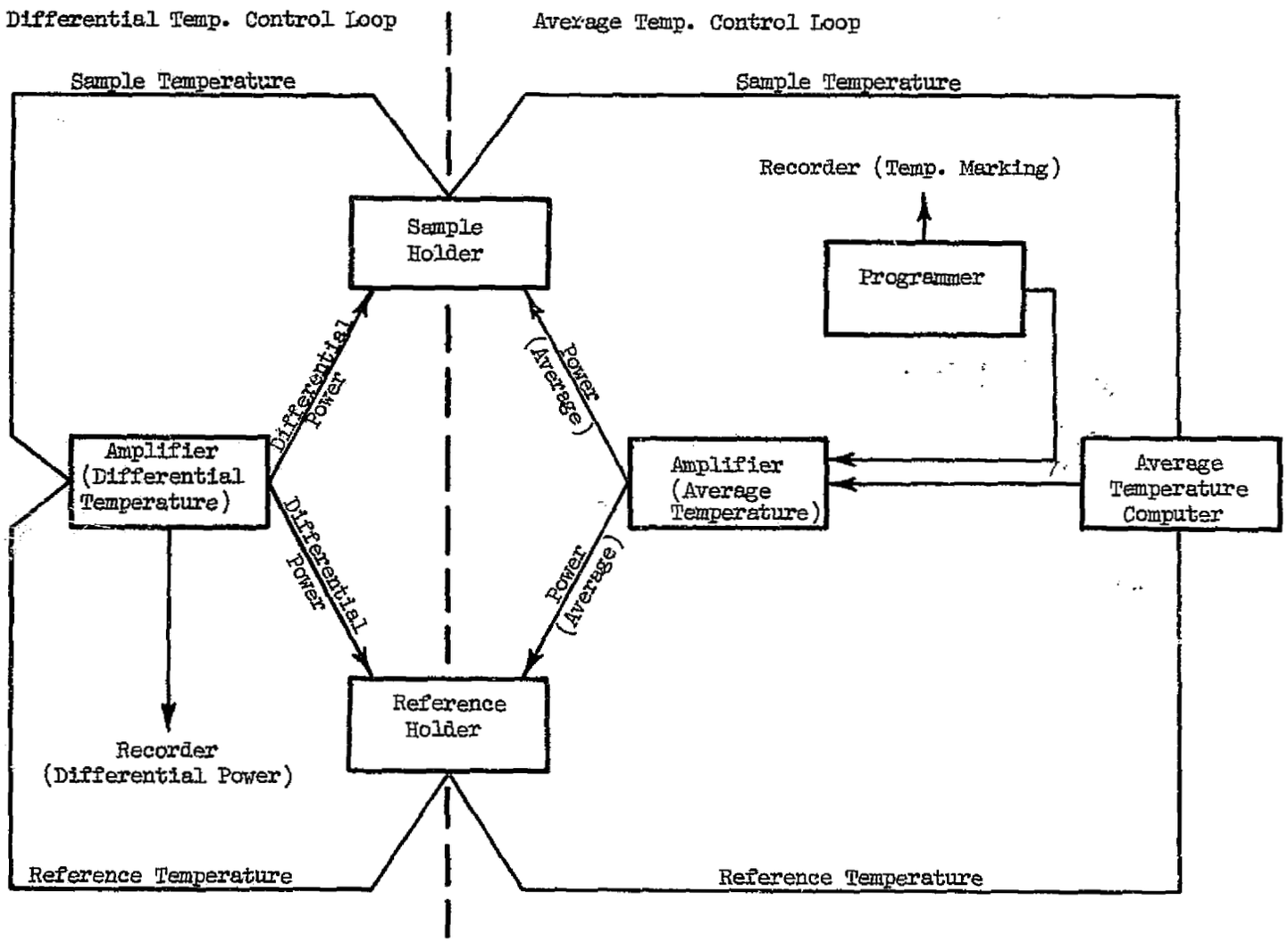

Figure 6.- DSC block diagram.

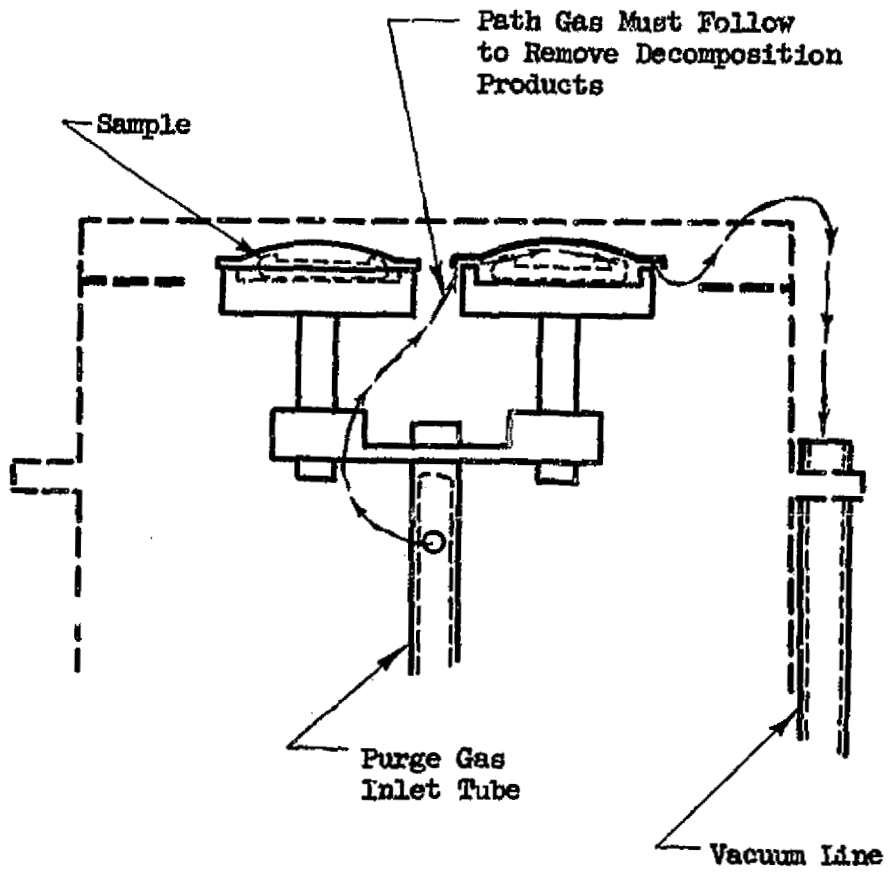

Figure 7.- DSC purge gas flow path schematic diagram.

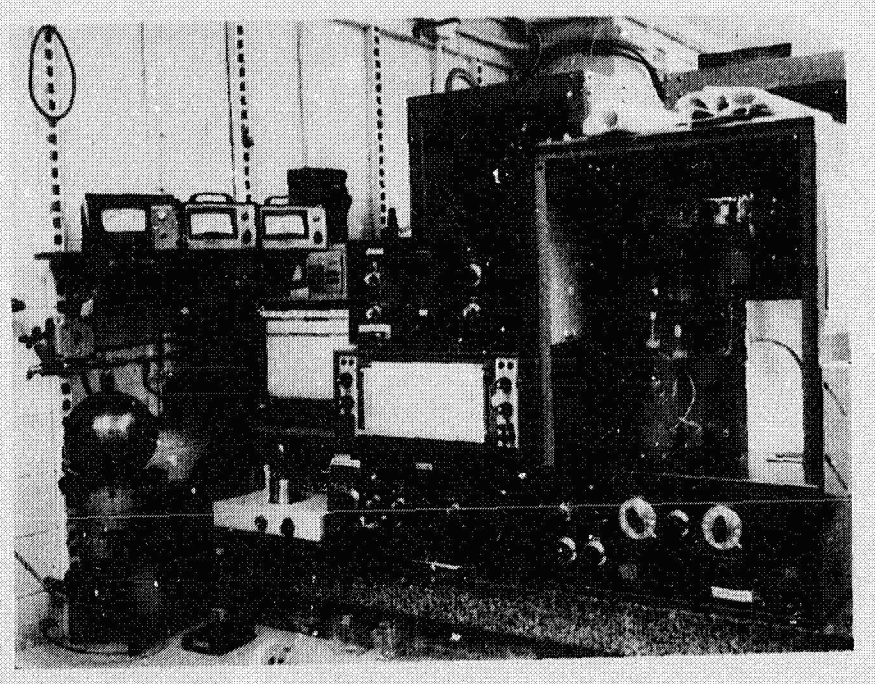

Figure 8.- DSC and TGA system.

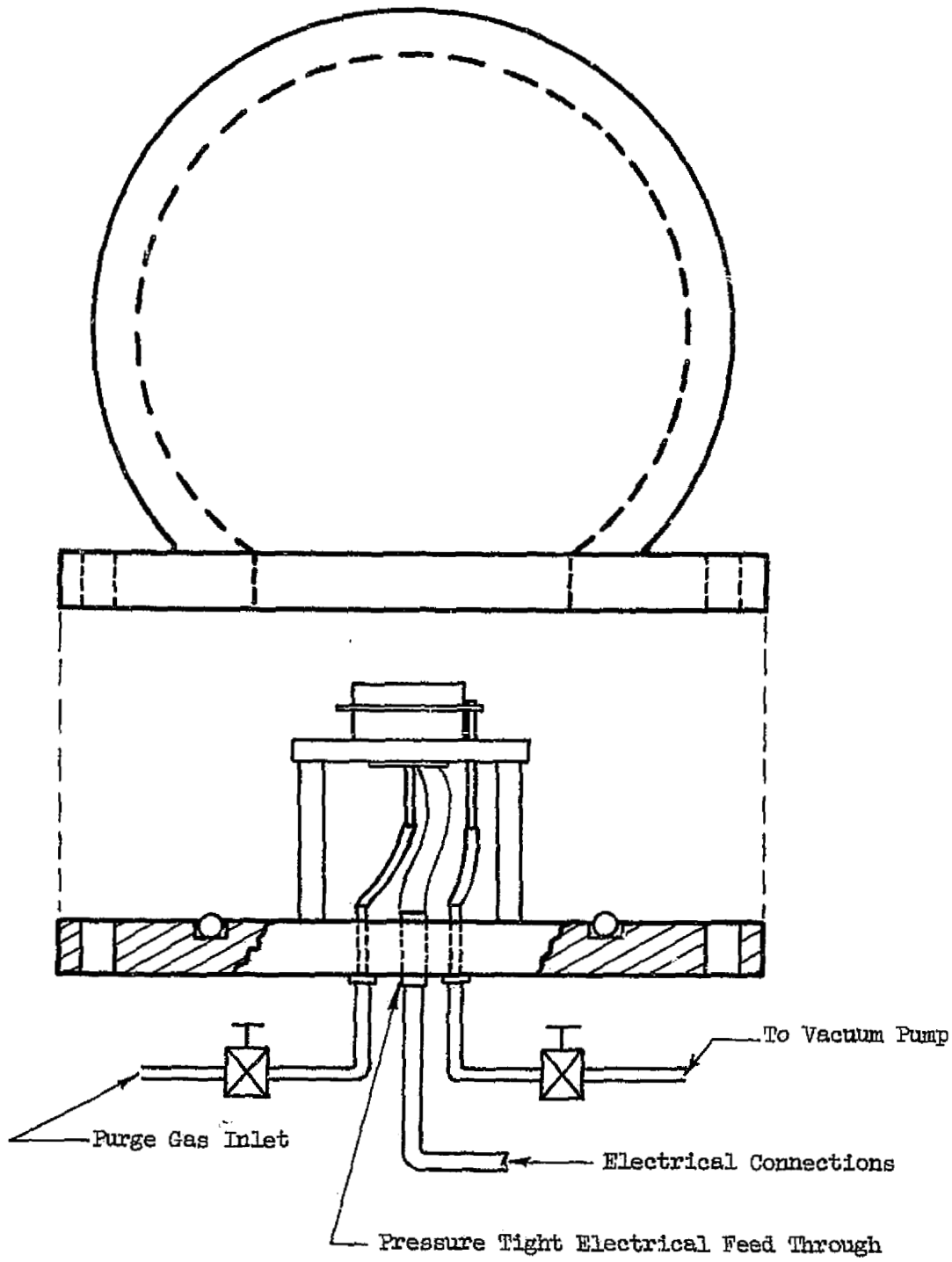

Figure 9.- DSC pressure vessel sketch.

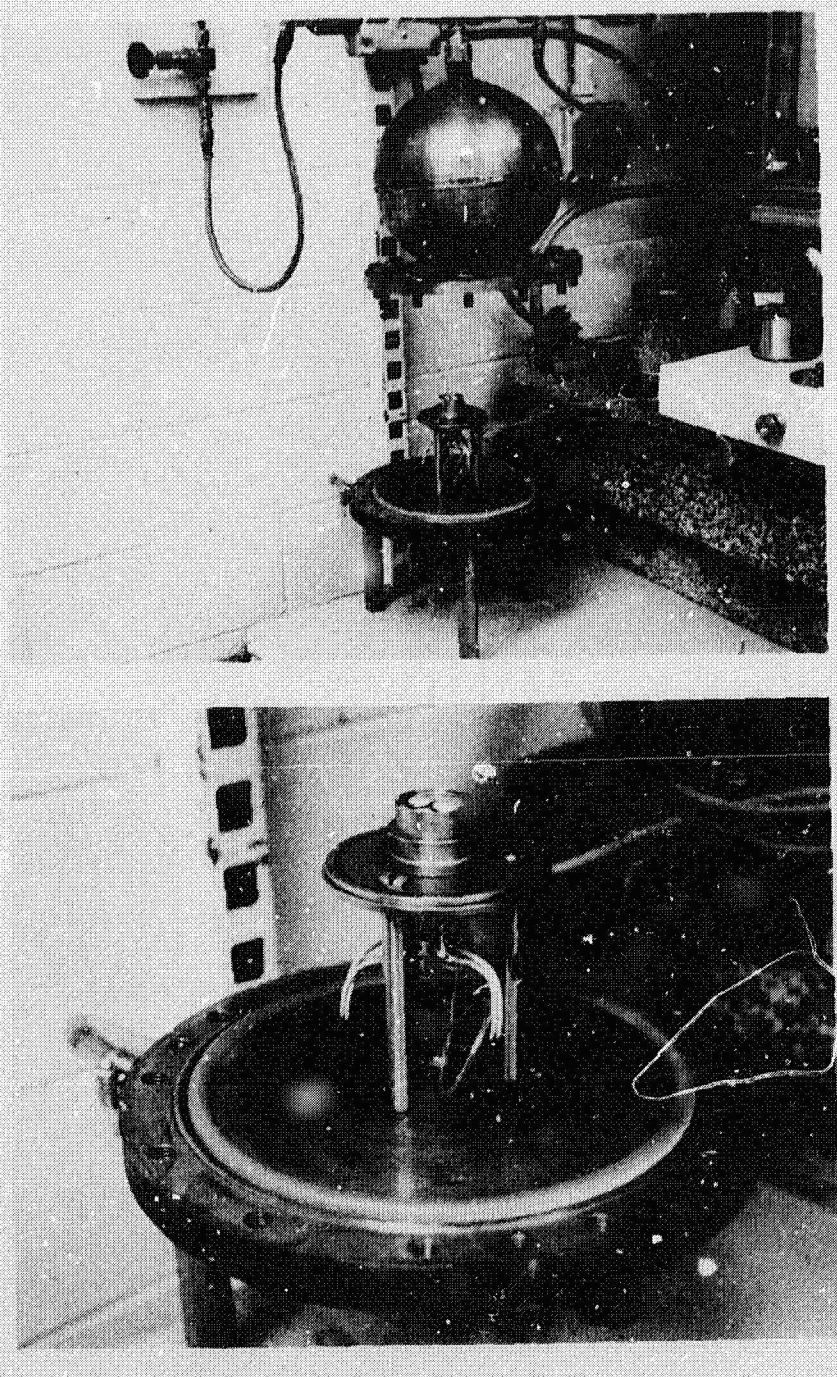

Figure 10.- DSC pressure vessel photographs.

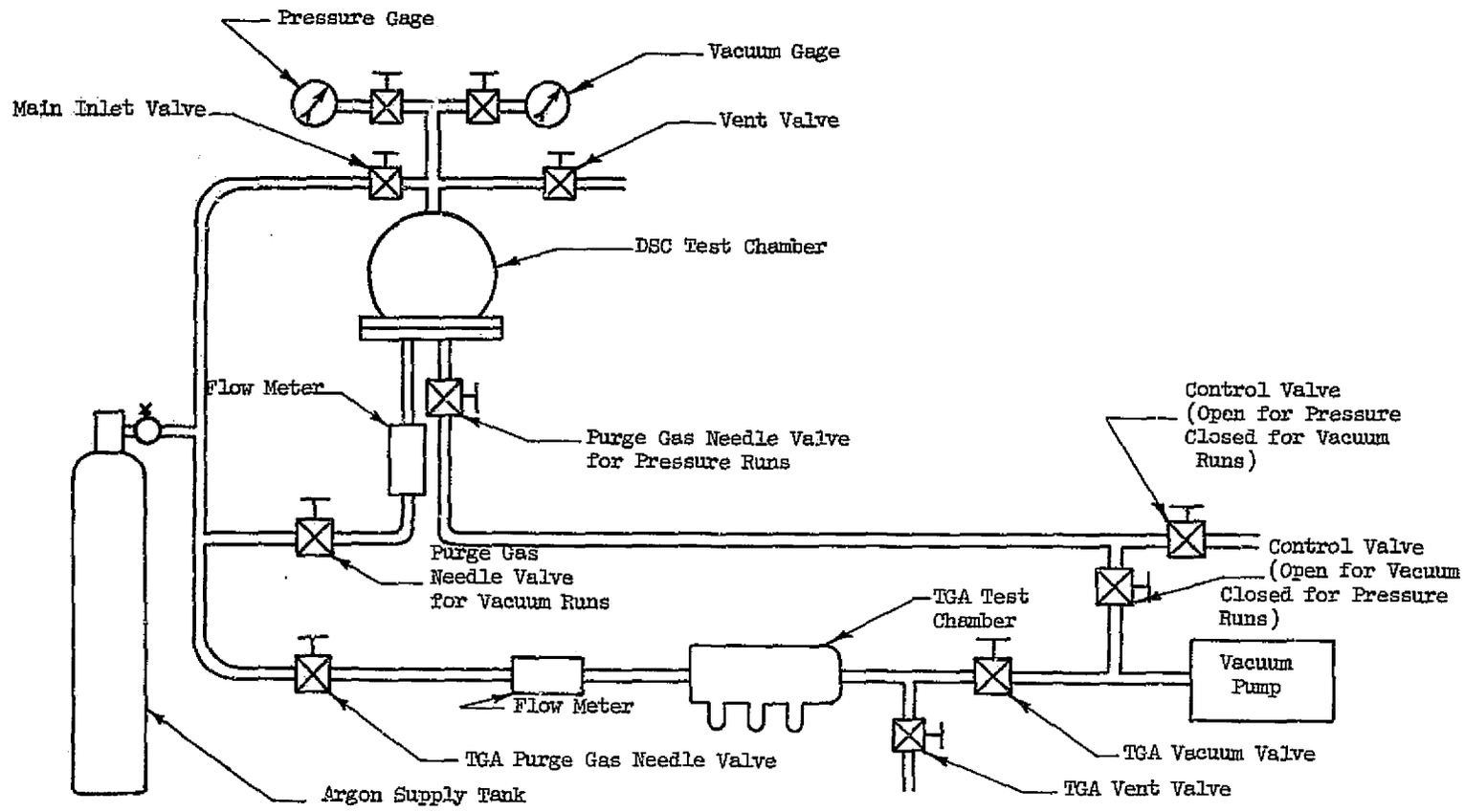

Figure 11.- DSC and TGA purge gas and vacuum system.

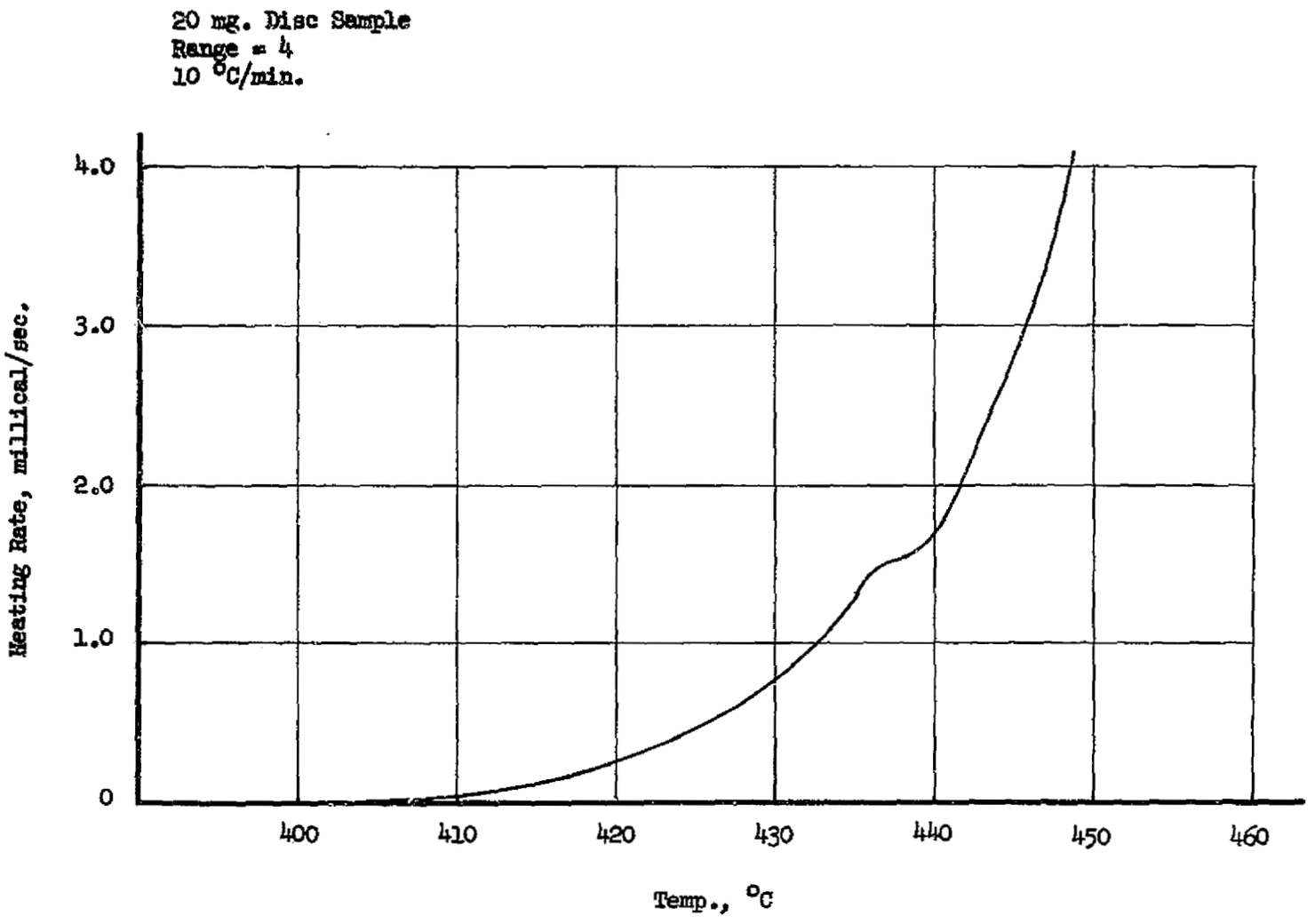

Figure 12.- DSC endothermic anomaly for M-2 propellant.

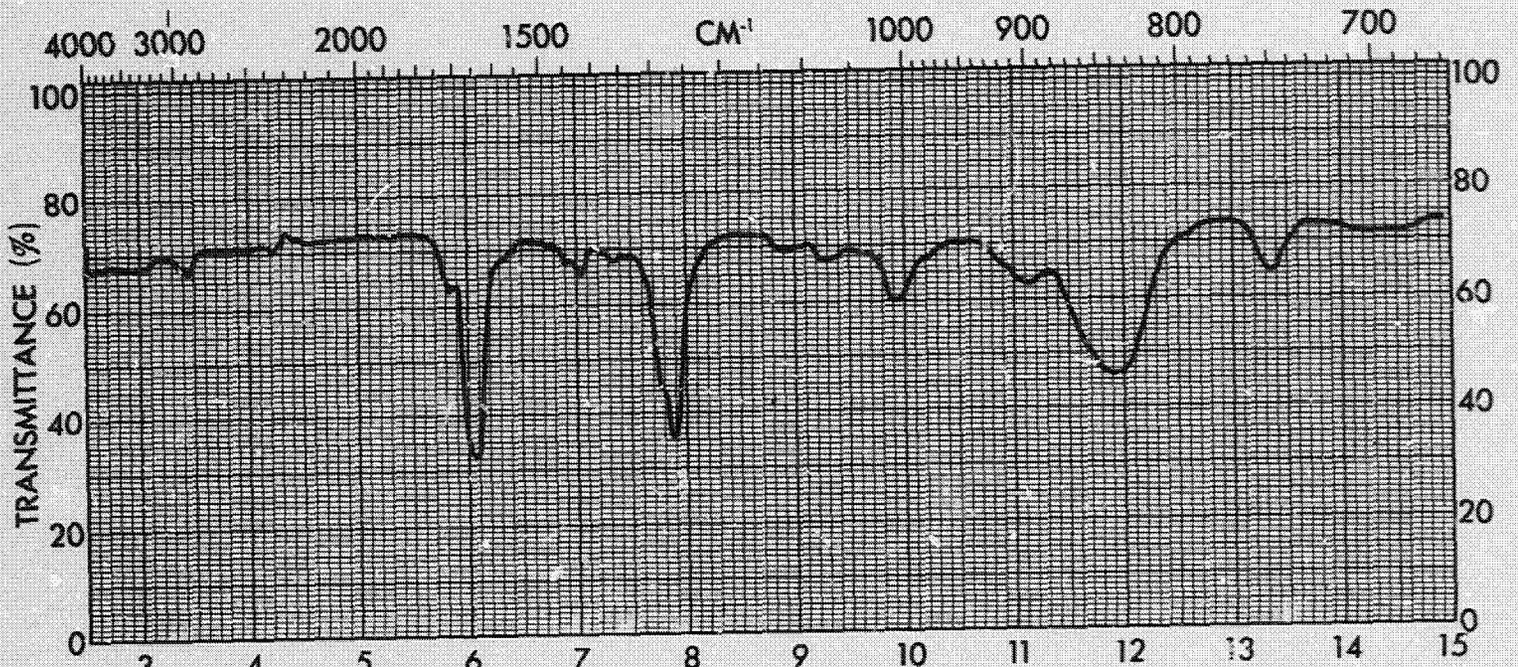

SPECTRUM NO.	ORIGIN Kirby	LEGEND	REMARKS Organic Nitrate: R-O-NO2
SAMPLE		1.	1) 1660-1625
	PURITY	2.	2) 1285-1270
	PHASE	DATE	3) 870-840
	THICKNESS	OPERATOR Kelliher	4) 760-745
			5) 712-690

SPECTRUM NO. SAMPLE

Figure 13.- Oily liquid infrared spectrum.

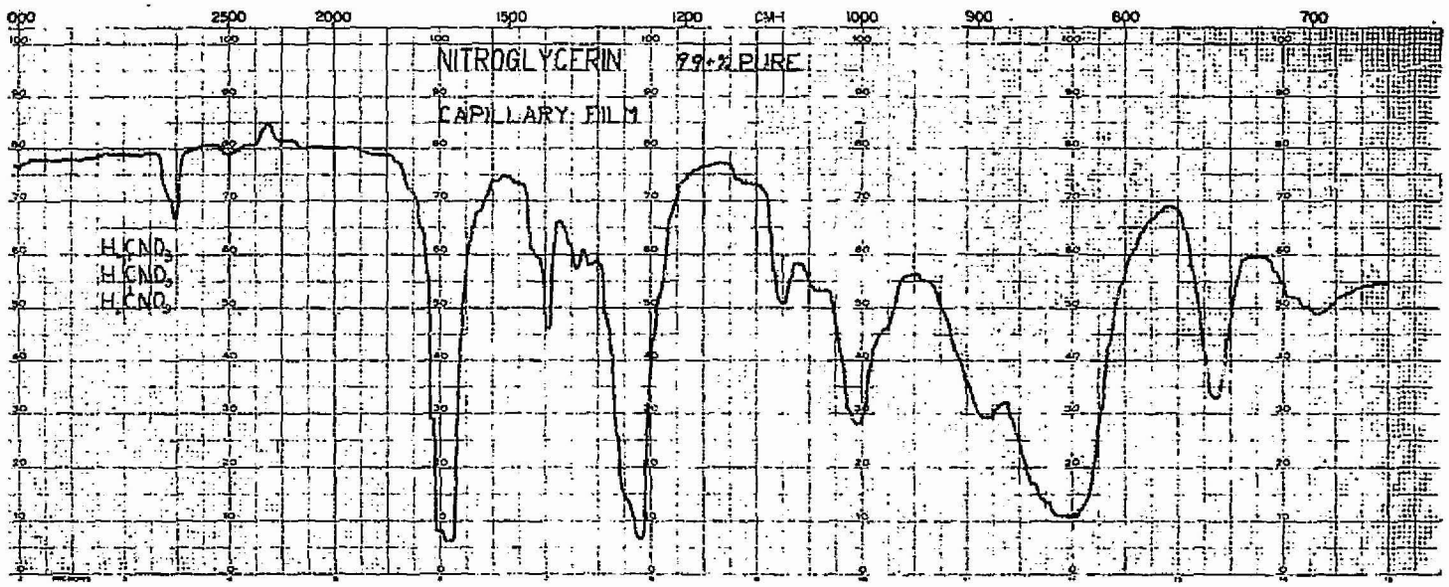

Figure 14.- Nitroglycerine infrared spectrum from Reference 34.

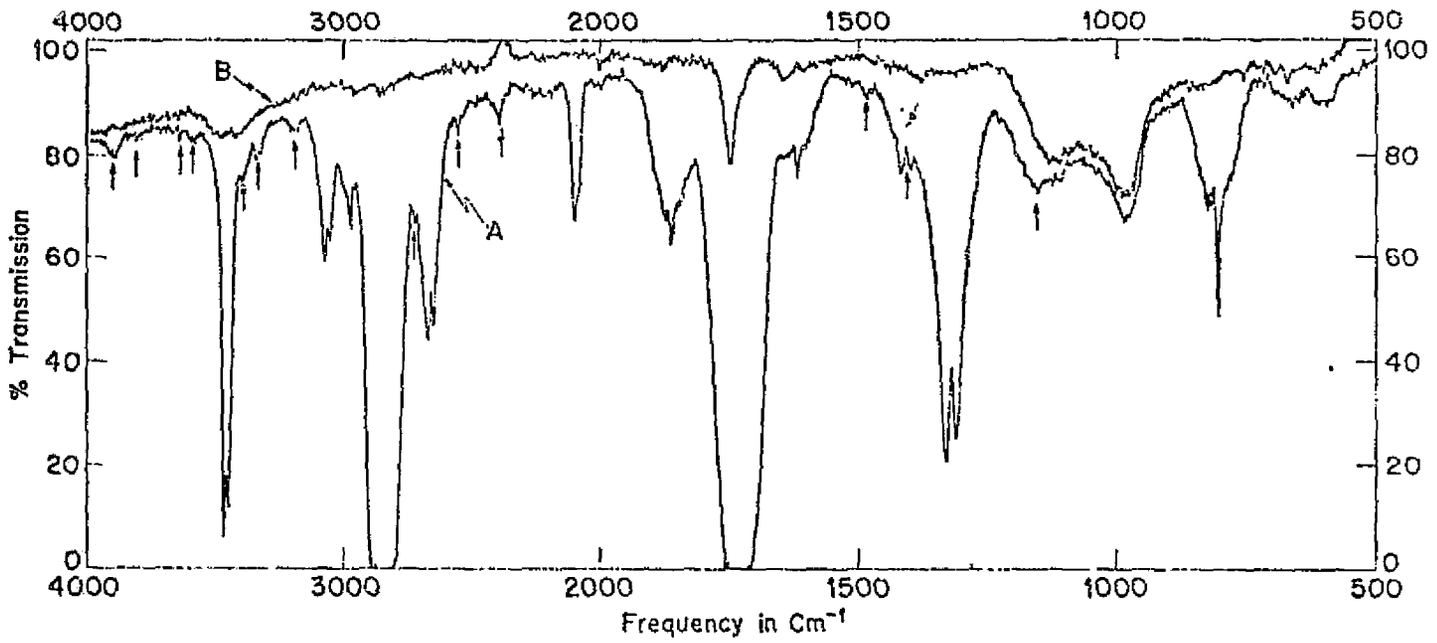

Figure 15.- Glyoxal infrared spectrum from Reference 35.

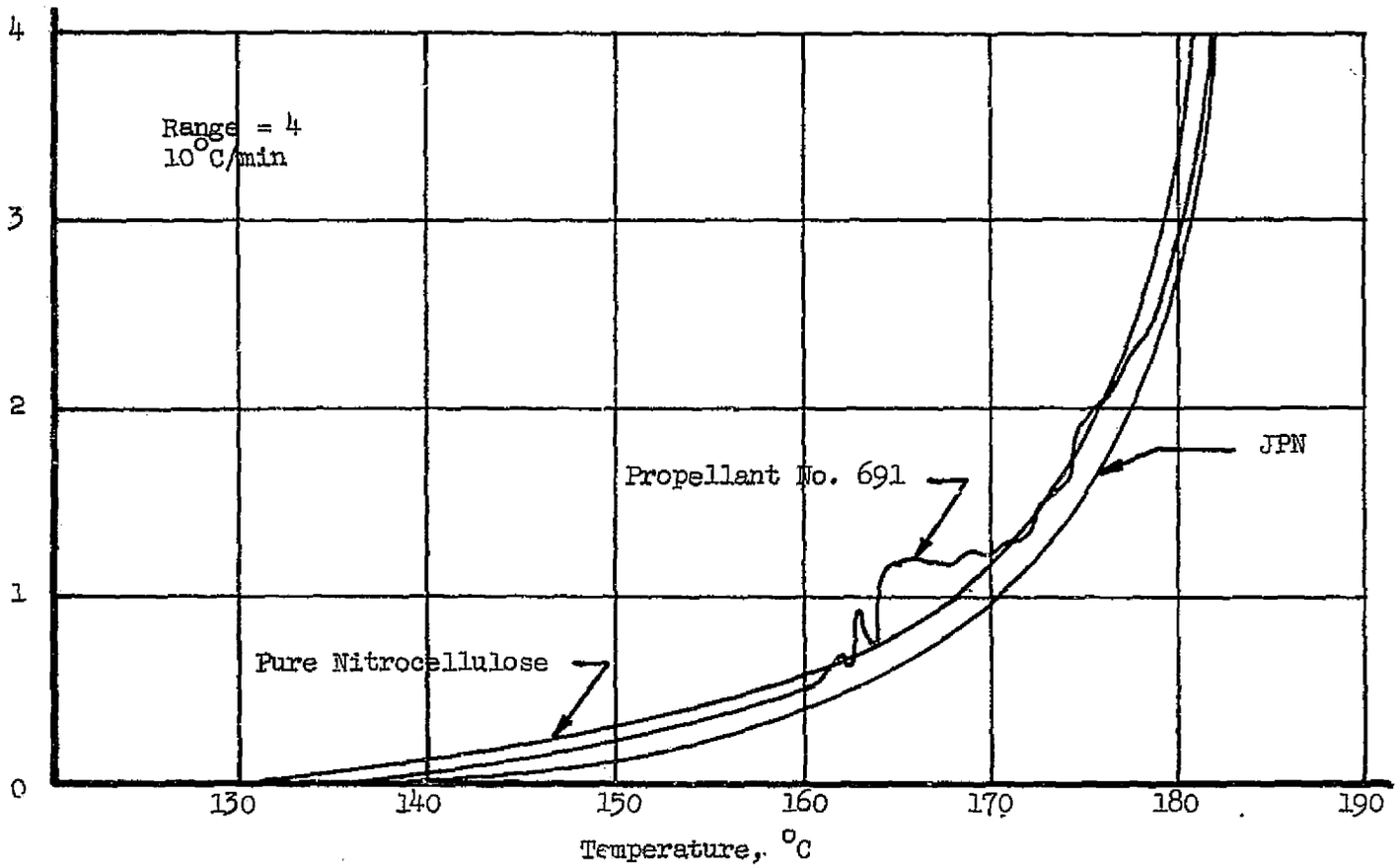

Figure 16.- DSC curves for pure nitrocellulose, JPN, and No. 691 propellants.

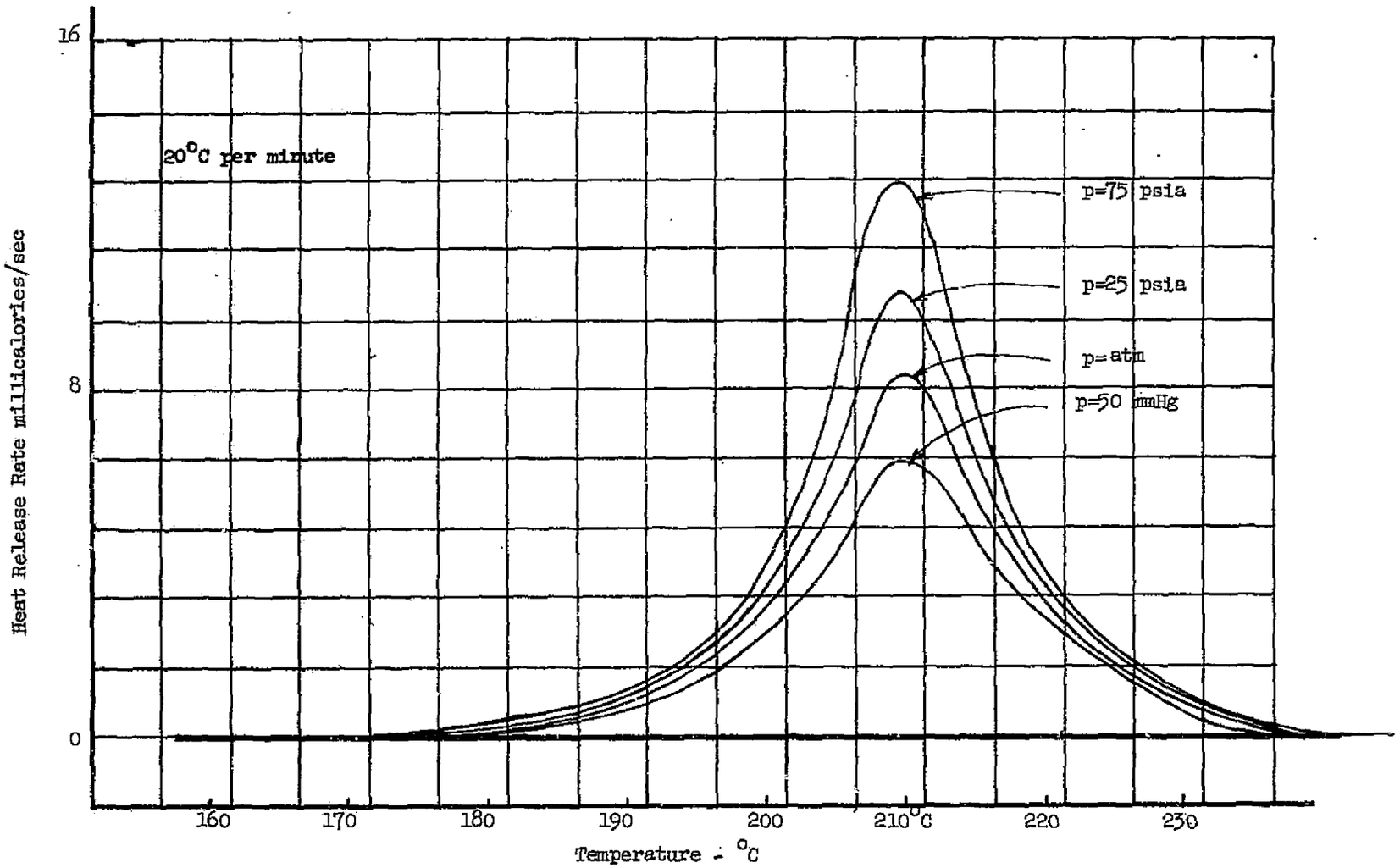

Figure 17.- Heat release rate versus pressure - 1 mg of M-2 in 9 mg of polyphenyl ether.

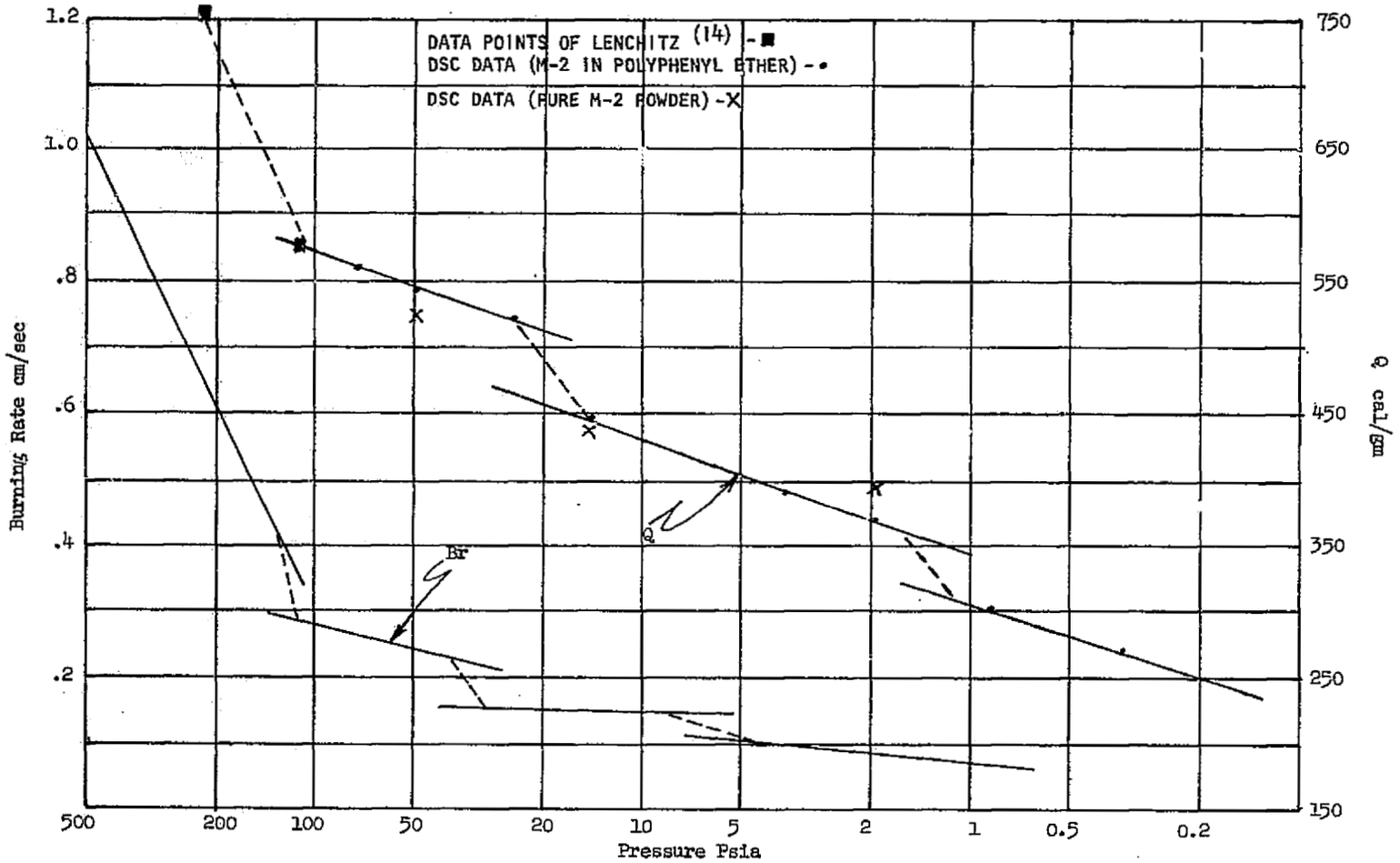

Figure 18.- Heat of reaction and burning rate versus pressure.

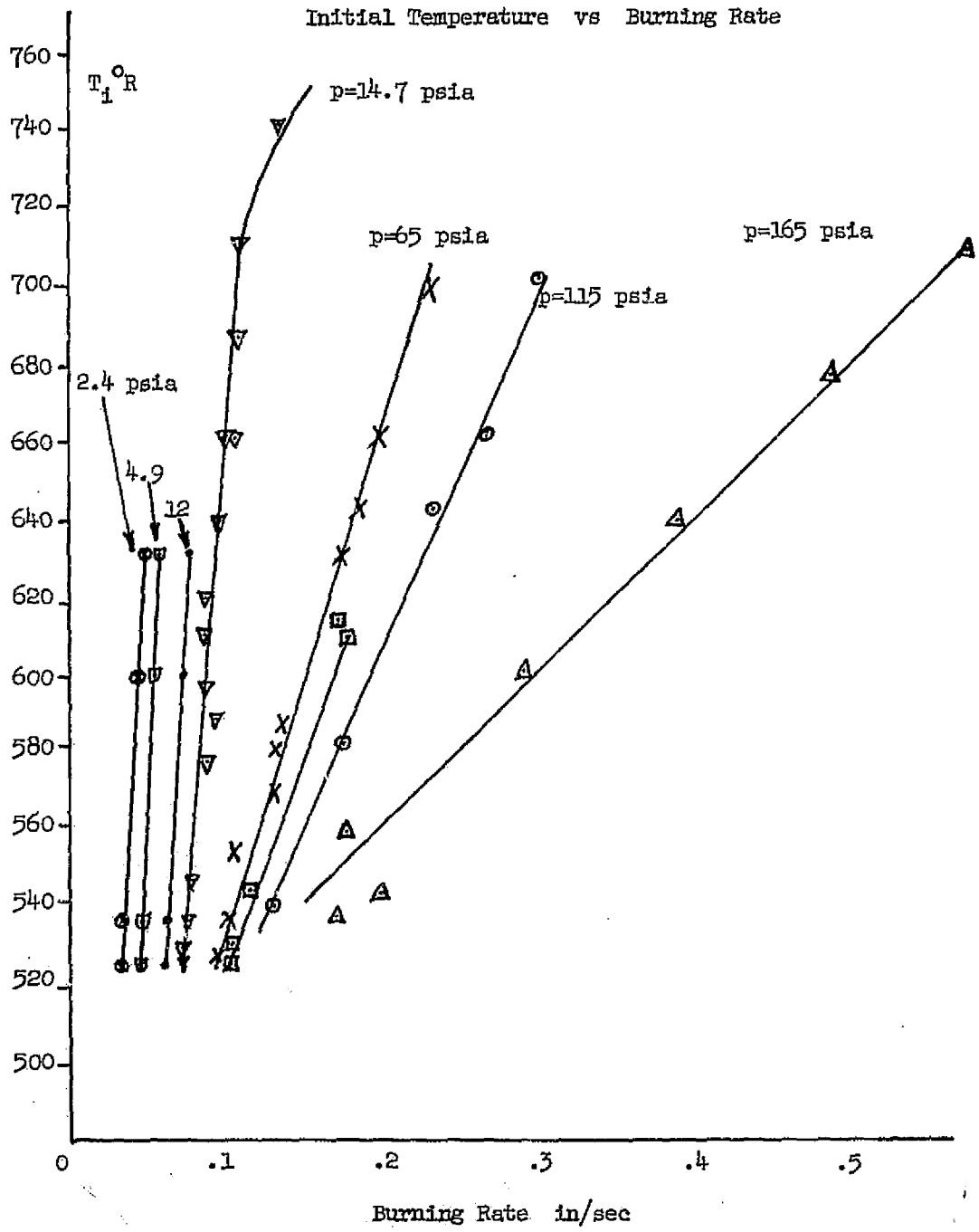

Figure 19.- Burning rate versus initial temperature (from ref. 24).

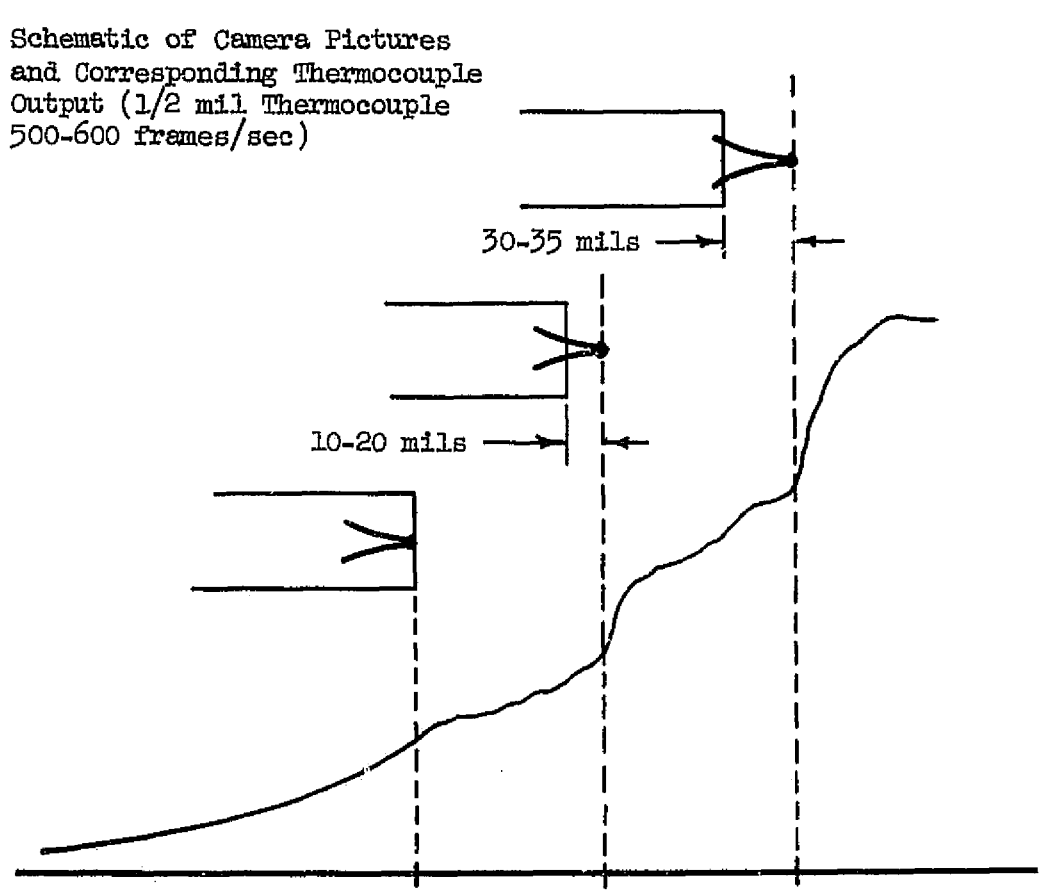

Figure 20.- Temperature jumps near surface (from ref. 10).

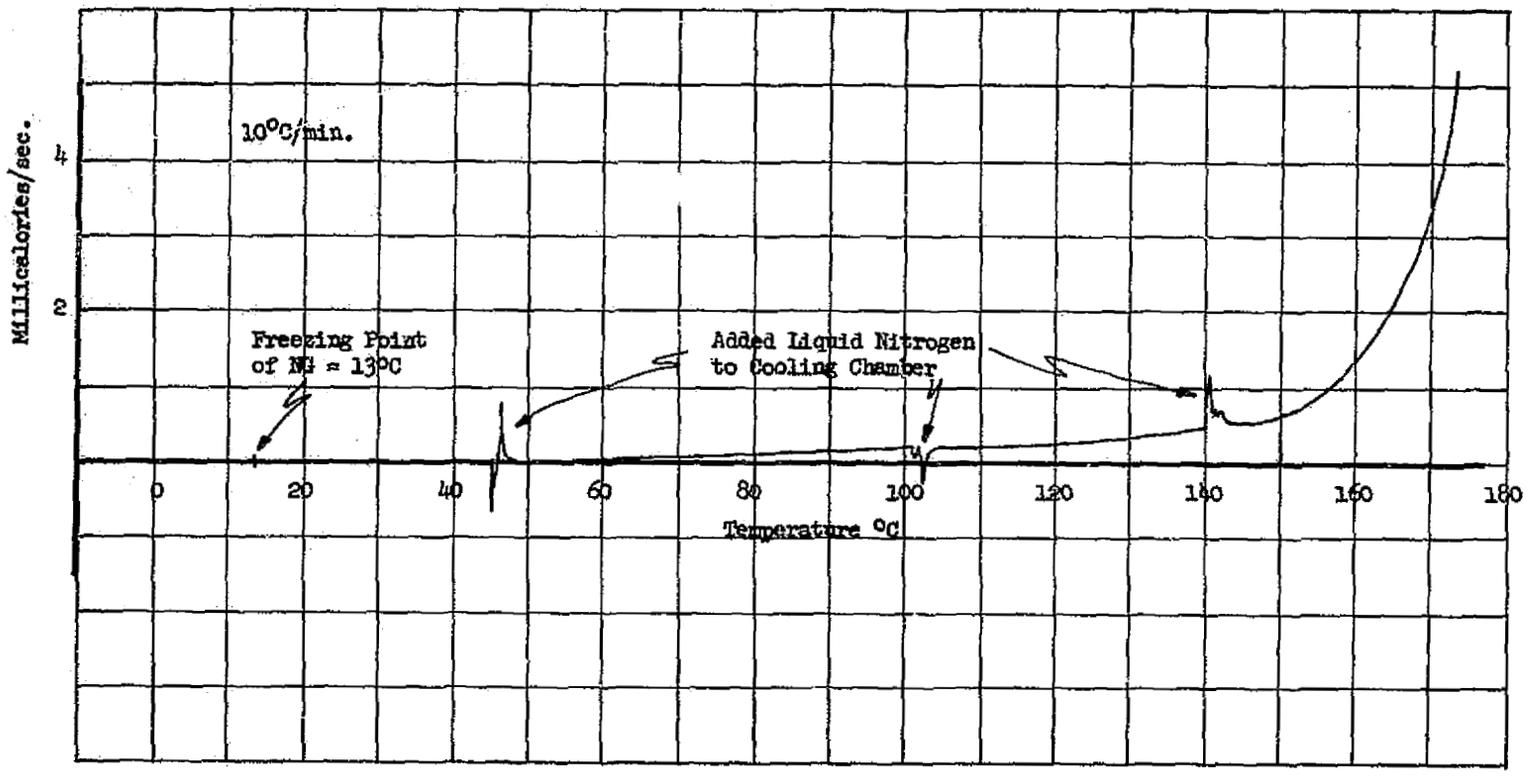

Figure 21.- Low-temperature DSC curve with LN_2 cooling.

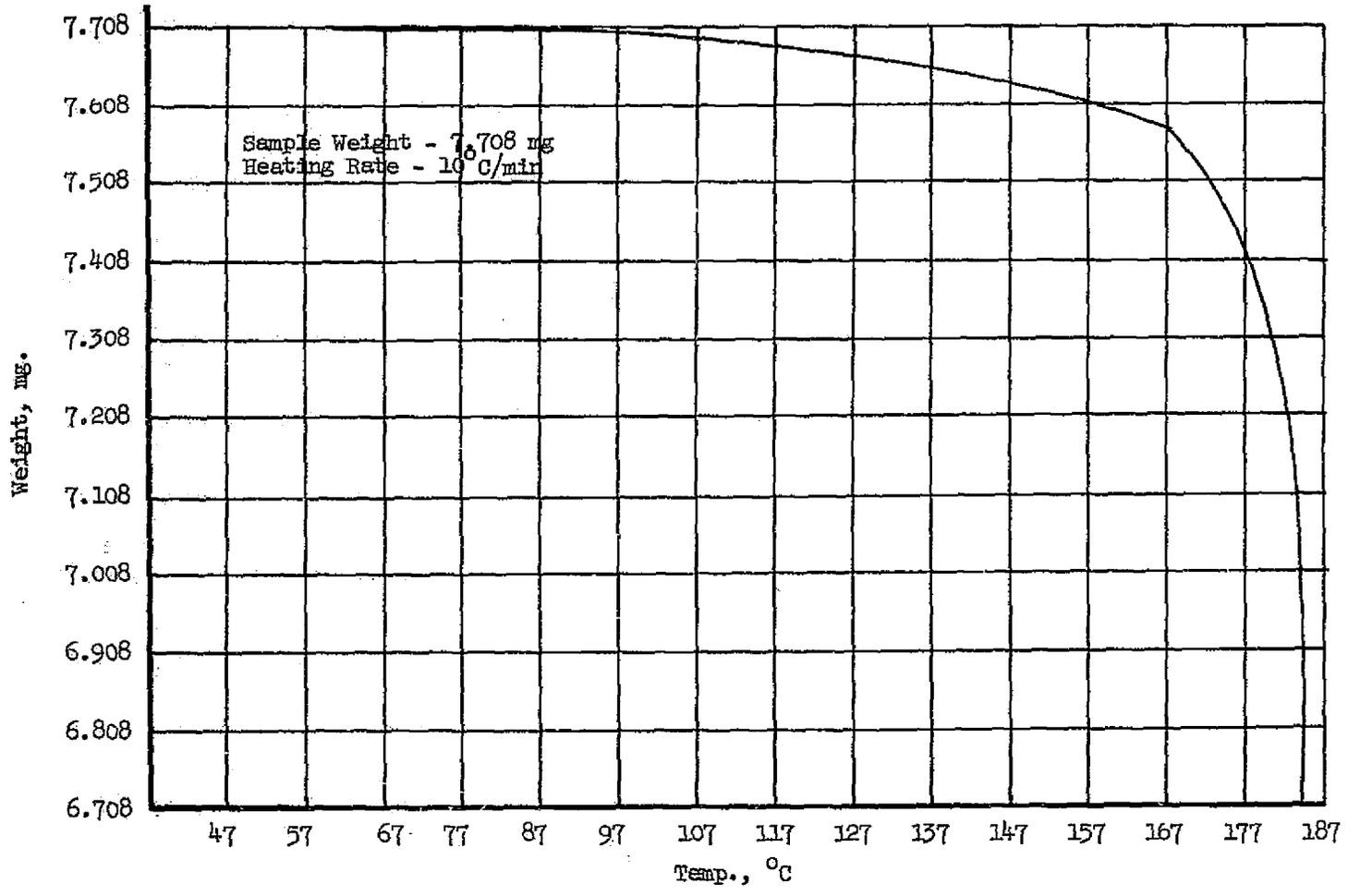

Figure 22.- TGA showing "knee" at same temperature as apparent endotherm DSC curve.

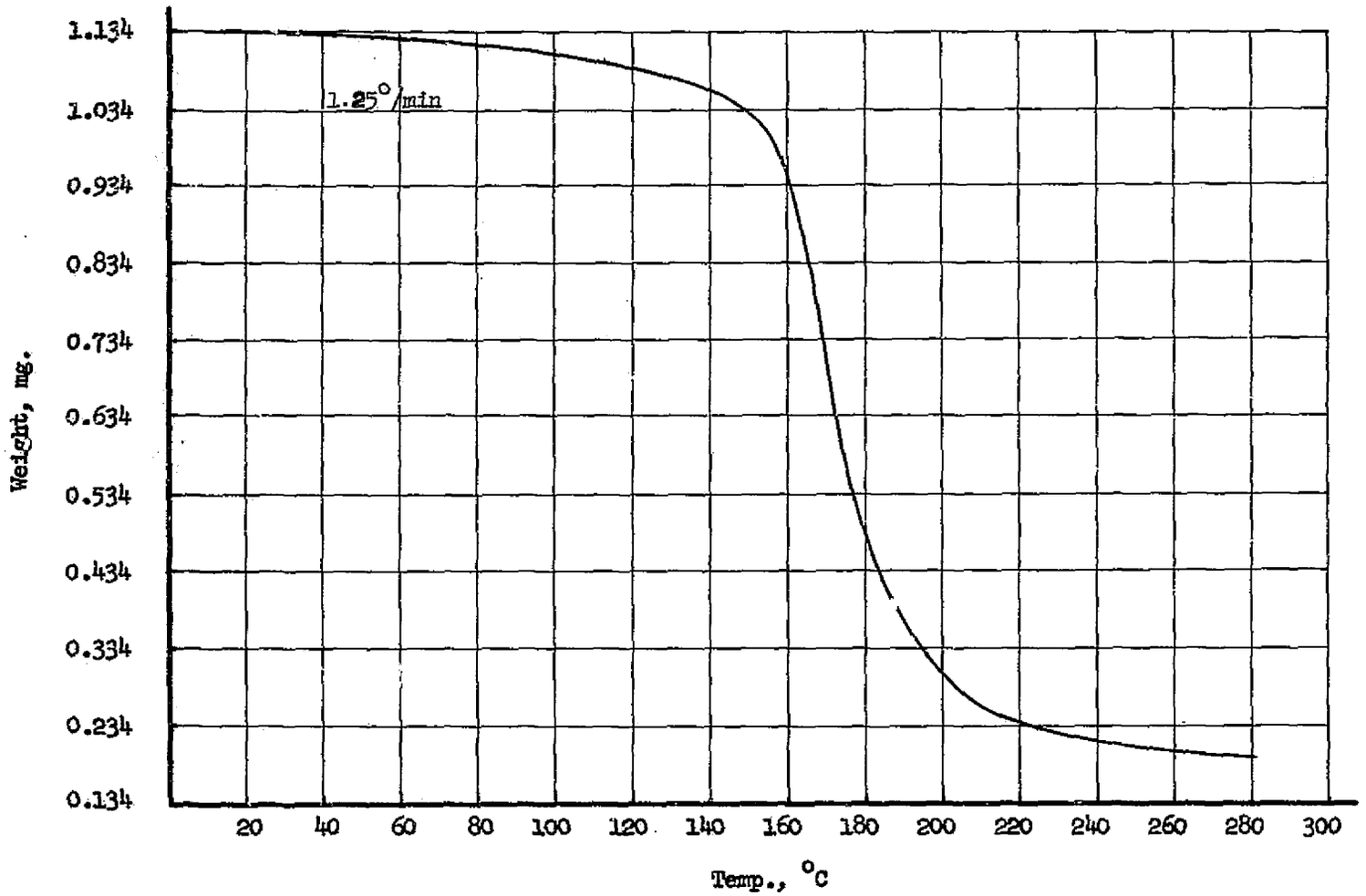

Figure 23.- Slow heating rate TGA curve which left carbonaceous residue.

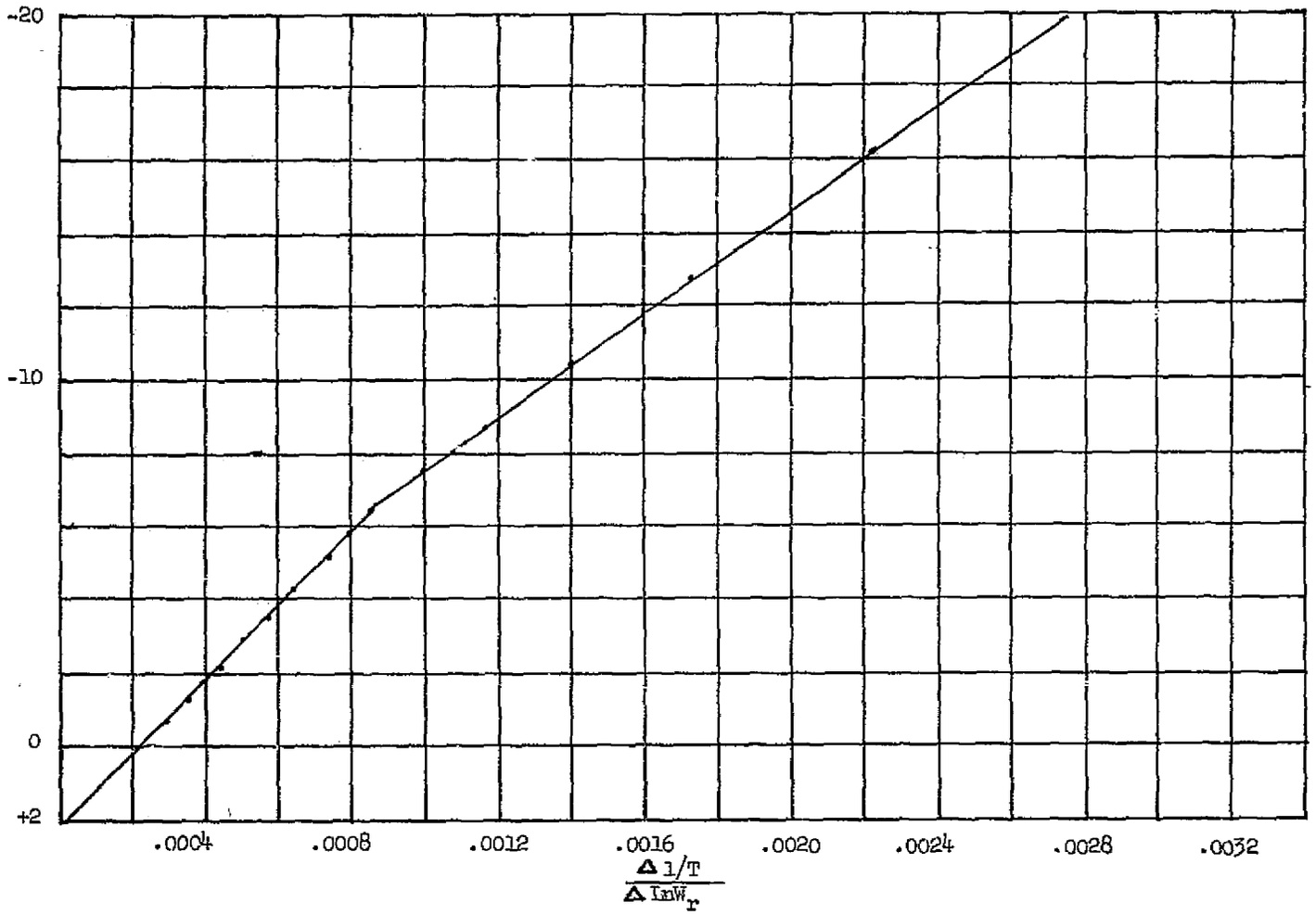

Figure 24.- Order of reaction curve by method of reference 23.

0.000	1.034	.984	1.96253906E+04	5.38299032E+07	-1.10359996E-01	5.84698785E-02
.200	1.034	.984	1.99339844E+04	8.30156496E+07	-3.13425073E-01	5.52433199E-02
.400	1.034	.984	2.02425781E+04	1.28011862E+08	-4.82224123E-01	5.74178050E-02
.600	1.034	.984	2.05589844E+04	1.99273886E+08	-6.59044452E-01	5.97919158E-02
.800	1.034	.984	2.08753906E+04	3.10173839E+08	-8.28981736E-01	6.20870266E-02
1.000	1.034	.984	2.11957031E+04	4.85055743E+08	-9.89452542E-01	6.93905754E-02
1.200	1.034	.984	2.15199219E+04	7.62095058E+08	-1.13708321E+00	7.55574934E-02
1.400	1.034	.984	2.18441406E+04	1.19724900E+09	-1.27579759E+00	8.19565839E-02
1.600	1.034	.984	2.21722656E+04	1.88969424E+09	-1.40458245E+00	8.83153537E-02
1.800	1.034	.984	2.25082031E+04	3.01092647E+09	-1.52288817E+00	9.44772918E-02
2.000	1.034	.984	2.28402344E+04	4.77417336E+09	-1.63283521E+00	1.00466315E-01
2.200	1.034	.984	2.31800781E+04	7.64181512E+09	-1.73362664E+00	1.06143668E-01
2.400	1.034	.984	2.35238281E+04	1.22892136E+10	-1.82662114E+00	1.11524439E-01
2.600	1.034	.984	2.38675781E+04	1.97612140E+10	-1.91305743E+00	1.16634775E-01
2.800	1.034	.984	2.42152344E+04	3.19251605E+10	-1.99317830E+00	1.21451256E-01
0.000	.984	.934	2.83480469E+04	2.22213915E+12	1.37295464E+00	1.07046555E-01
.200	.984	.934	2.89886719E+04	5.10294363E+12	1.18980478E+00	9.43292481E-02
.400	.984	.934	2.96410156E+04	1.18816380E+13	1.01339692E+00	8.25505967E-02
.600	.984	.934	3.02972656E+04	2.77882940E+13	8.34894399E-01	7.05170829E-02
.800	.984	.934	3.09691406E+04	6.62048071E+13	6.64281979E-01	5.93985837E-02
1.000	.984	.934	3.16449219E+04	1.58434485E+14	5.01056604E-01	4.92087658E-02
1.200	.984	.934	3.23324219E+04	3.84427393E+14	3.44644841E-01	3.99955456E-02
1.400	.984	.934	3.30316406E+04	9.45761232E+14	1.96394093E-01	3.21386222E-02
1.600	.984	.934	3.37386719E+04	2.34810660E+15	5.70439892E-02	2.62168260E-02
1.800	.984	.934	3.44535156E+04	5.88334750E+15	-7.33244545E-02	2.29310197E-02
2.000	.984	.934	3.51800781E+04	1.49462641E+16	-1.94676111E-01	2.26493317E-02
2.200	.984	.934	3.59144531E+04	3.83187904E+16	-3.07764038E-01	2.48659124E-02
2.400	.984	.934	3.66566406E+04	9.91432450E+16	-4.13099746E-01	2.85802876E-02
2.600	.984	.934	3.74105469E+04	2.60084838E+17	-5.10957365E-01	3.29724897E-02
2.800	.984	.934	3.81761719E+04	6.91777006E+17	-6.01923335E-01	3.75803886E-02
1.687	.984	.934	3.40472656E+04	3.49165779E+15	-9.25256915E-04	2.44229388E-02
0.000	.934	.884	2.68441406E+04	3.63521398E+11	1.22302548E+00	9.86497439E-02
.200	.934	.884	2.76644531E+04	1.03779817E+12	1.04761773E+00	8.58368620E-02
.400	.934	.884	2.85042969E+04	3.03044636E+12	8.91012930E-01	7.52353884E-02
.600	.934	.884	2.93558594E+04	8.96965451E+12	7.40321567E-01	6.53238118E-02
.800	.934	.884	3.02269531E+04	2.71626966E+13	5.92021705E-01	5.55960611E-02
1.000	.934	.884	3.11136719E+04	8.37660157E+13	4.51131025E-01	4.67676369E-02
1.200	.934	.884	3.20195219E+04	2.64298545E+14	3.16225399E-01	3.87514988E-02
1.400	.934	.884	3.29378906E+04	8.45276618E+14	1.88206650E-01	3.18441601E-02
1.600	.934	.884	3.38715390E+04	2.76583122E+15	6.85821451E-02	2.64858731E-02
1.800	.934	.884	3.48285156E+04	9.21627353E+15	-4.28779499E-02	2.30907314E-02
2.000	.934	.884	3.57572656E+04	3.12743961E+16	-1.46446164E-01	2.19255676E-02
2.200	.934	.884	3.67816406E+04	1.08075545E+17	-2.42530410E-01	2.27994279E-02
2.400	.934	.884	3.77855469E+04	3.82107349E+17	-3.31406281E-01	2.50975781E-02
2.600	.934	.884	3.88056781E+04	1.37577726E+18	-4.13814595E-01	2.81914795E-02
2.800	.934	.884	3.98382812E+04	5.03281607E+18	-4.90365960E-01	3.16481069E-02
1.724	.934	.884	3.44652344E+04	5.82576011E+15	-1.31387466E-03	2.41290859E-02

Figure 25.- Computer printout near "knee" of curve.

C.000	.784	.734	2.67230469E+04	3.04520765E+11	1.05990106E+00	9.10853285E-02
.200	.784	.734	2.83246C94E+C4	2.19630885E+12	9.39221666E-01	8.35061724E-02
.400	.784	.734	2.99886719E+04	1.70165486E+13	8.26316715E-01	7.65376637E-02
.600	.784	.734	3.171514C6E+04	1.42278435E+14	7.15745075E-01	6.95902880E-02
.800	.784	.734	3.35121094E+04	1.27790544E+15	6.10149767E-01	6.30715754E-02
1.000	.784	.734	3.53675781E+04	1.23296796E+16	5.09859797E-01	5.69799021E-02
1.200	.784	.734	3.72894531E+C4	1.28376357E+17	4.14598618E-01	5.13780803E-02
1.400	.784	.734	3.92757812E+04	1.43914604E+18	3.24850438E-01	4.63348993E-02
1.600	.784	.734	4.133046E7E+C4	1.74498998E+19	2.41276232E-01	4.19316324E-02
1.800	.784	.734	4.34398437E+04	2.25228321E+20	1.63874450E-01	3.81729647E-02
2.000	.784	.734	4.56195312E+04	3.15149568E+21	9.26198847E-02	3.50901271E-02
2.200	.784	.734	4.78617187E+04	4.73718277E+22	2.70991238E-02	3.26447001E-02
2.400	.784	.734	5.01664062E+04	7.64960391E+23	-3.30790372E-02	3.07982341E-02
2.600	.784	.734	5.25257812E+C4	1.31502809E+25	-8.83935674E-02	2.94867775E-02
2.800	.784	.734	5.49554687E+04	2.45077258E+26	-1.39103668E-01	2.86691713E-02
2.290	.784	.734	4.88851562E+C4	1.63015666E+23	-4.98393885E-04	3.17448222E-02
C.000	.534	.484	1.16869141E+04	5.55020573E+03	1.98665485E+00	1.05901496E-01
.200	.534	.484	1.34935547E+04	5.43931446E+04	1.67159785E+00	9.09841819E-02
.400	.534	.484	1.54837891E+04	6.54913000E+05	1.40860042E+00	7.87104295E-02
.600	.534	.484	1.76615234E+C4	9.72908323E+06	1.18135513E+00	6.82386405E-02
.800	.534	.484	2.00355469E+04	1.80125453E+08	9.83631271E-01	5.88876729E-02
1.000	.534	.484	2.26015631E+04	4.13674682E+09	8.07082024E-01	5.07002931E-02
1.200	.534	.484	2.53675781E+04	1.18783989E+11	6.49884842E-01	4.38758577E-02
1.400	.534	.484	2.83285156E+C4	4.24539263E+12	5.09662330E-01	3.75382911E-02
1.600	.534	.484	3.14847656E+04	1.88874425E+14	3.83649996E-01	3.26033568E-02
1.800	.534	.484	3.48246094E+04	1.03213095E+16	2.70400781E-01	2.88573960E-02
2.000	.534	.484	3.8348C469E+04	6.92909495E+17	1.67941083E-01	2.63657966E-02
2.200	.534	.484	4.20492187E+04	5.67747378E+19	7.49324065E-02	2.51518580E-02
2.400	.534	.484	4.59085937E+04	5.55355835E+21	-9.15035042E-03	2.51109370E-02
2.600	.534	.484	4.99320312E+04	6.52984414E+23	-8.59561946E-02	2.60235183E-02
2.800	.534	.484	5.40962537E+C4	8.98752711E+25	-1.55650732E-01	2.76060815E-02
2.382	.534	.484	4.55570312E+04	3.65869593E+21	-2.10717632E-03	2.50750526E-02
0.000	.334	.284	1.55153809E+03	1.63811681E-02	9.04461062E+00	4.83707361E-01
.200	.334	.284	2.43630371E+03	6.72111311E-02	8.02100780E+CC	4.22165026E-01
.400	.334	.284	3.575E3CC8E+03	3.62400755E-01	6.41073917E+00	3.36665450E-01
.600	.334	.284	4.99794922E+03	2.64636225E+00	5.13795477E+C0	2.75282462E-01
.800	.334	.284	6.72646484E+03	2.68556044E+01	4.19224578E+00	2.30636081E-01
1.000	.334	.284	8.77626953E+03	3.84025895E+02	3.45559811E+00	1.95862040E-01
1.200	.334	.284	1.11517578E+C4	7.82223231E+03	2.85944013E+00	1.67324929E-01
1.400	.334	.284	1.38451172E+04	2.23622668E+05	2.36403878E+00	1.43068623E-01
1.600	.334	.284	1.68373047E+04	8.80811827E+06	1.94523741E+C0	1.22014387E-01
1.800	.334	.284	2.01056594E+C4	4.66671064E+08	1.58629652E+00	1.03485300E-01
2.000	.334	.284	2.36175781E+04	3.20902062E+10	1.27671090E+00	8.71728839E-02
2.200	.334	.284	2.73324219E+04	2.74311034E+12	1.01011686E+00	7.29539357E-02
2.400	.334	.284	3.12230469E+C4	2.83117431E+14	7.78872725E-01	6.06179595E-02
2.600	.334	.284	3.525C39C6E+04	3.38285781E+16	5.79655902E-01	5.01696467E-02
2.800	.334	.284	3.93925687E+04	4.57340165E+18	4.07004279E-01	4.14996805E-02

Figure 26.- Computer printout along second-order part of curve.

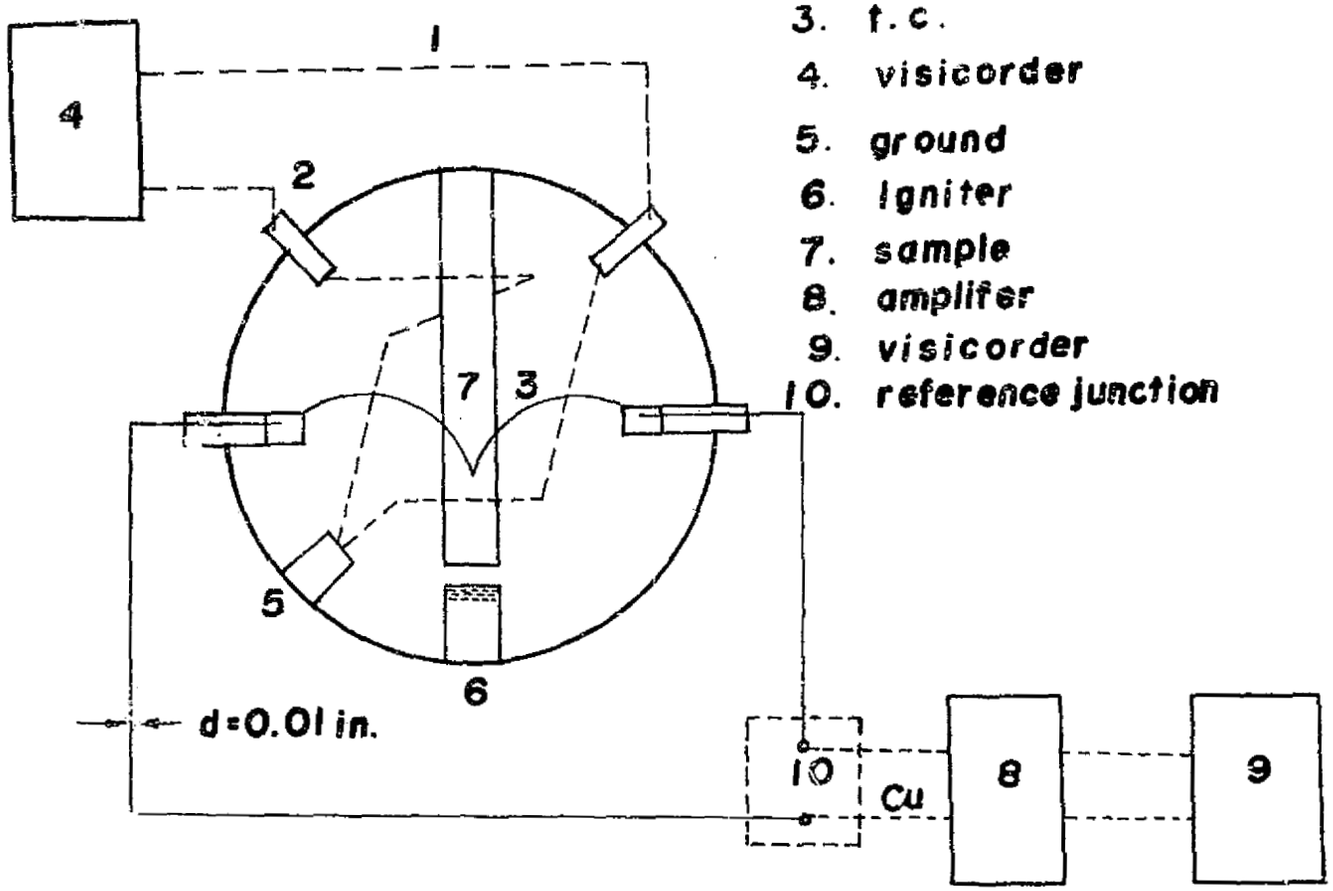

1. 1st fuse wire
2. 2nd "
3. t.c.
4. visicorder
5. ground
6. igniter
7. sample
8. amplifer
9. visicorder
10. reference junction

Figure 27.- System for autoignition measurements of reference 24.

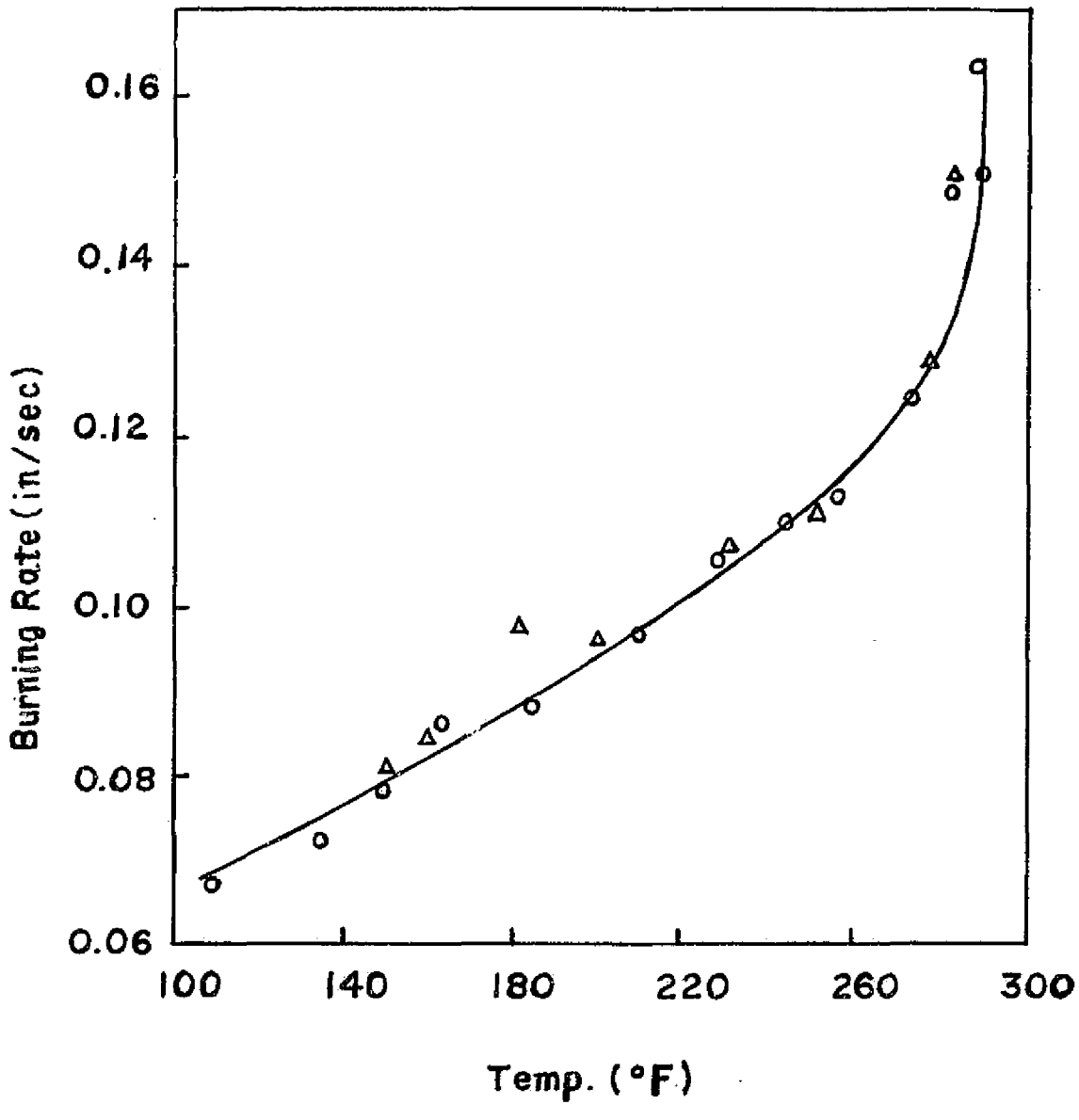

Figure 28.- Burning rate versus initial temperature (from ref. 24)

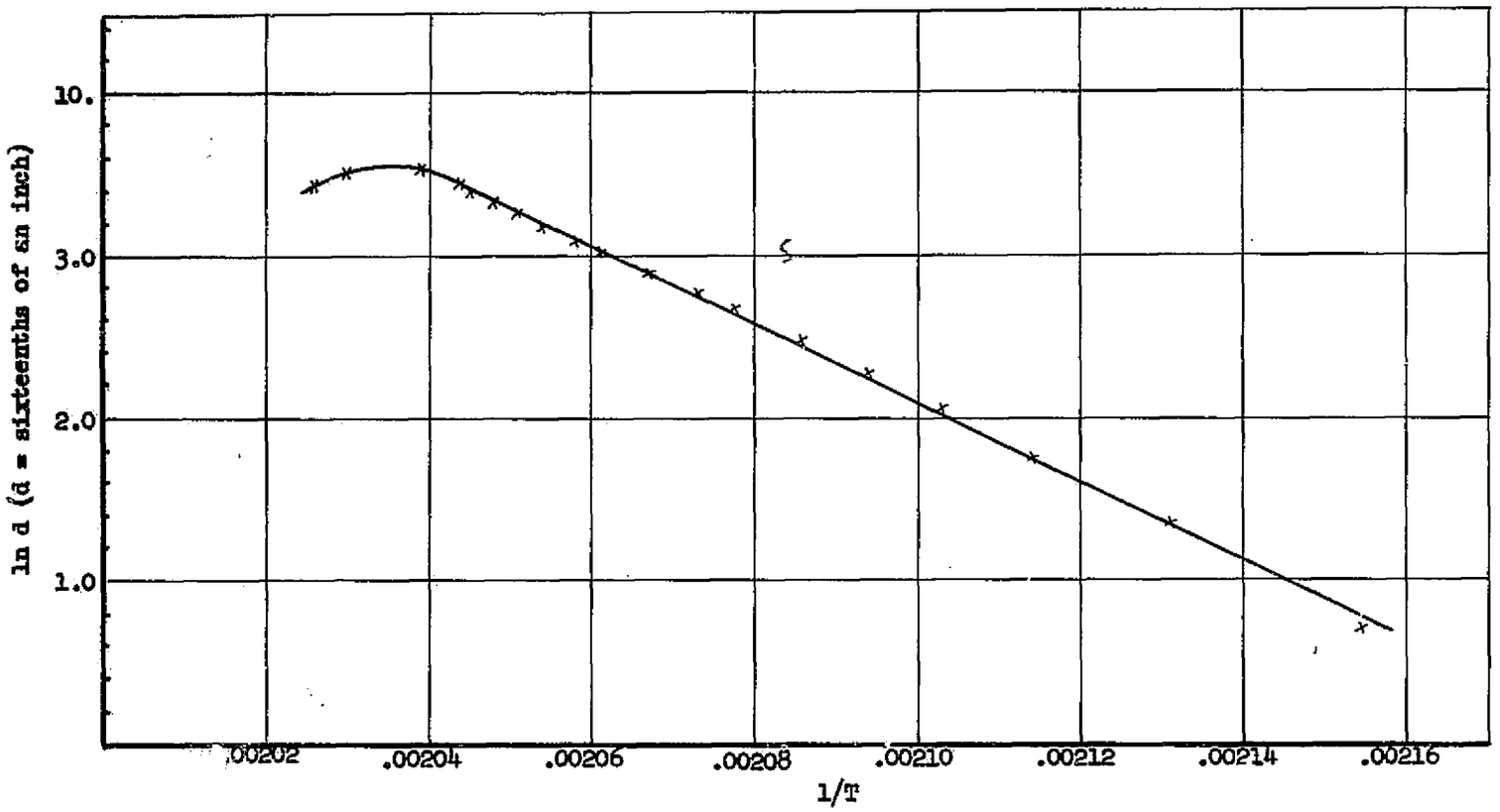

Figure 29.- Arrhenius plot of 50 mm Hg curve of figure 16.

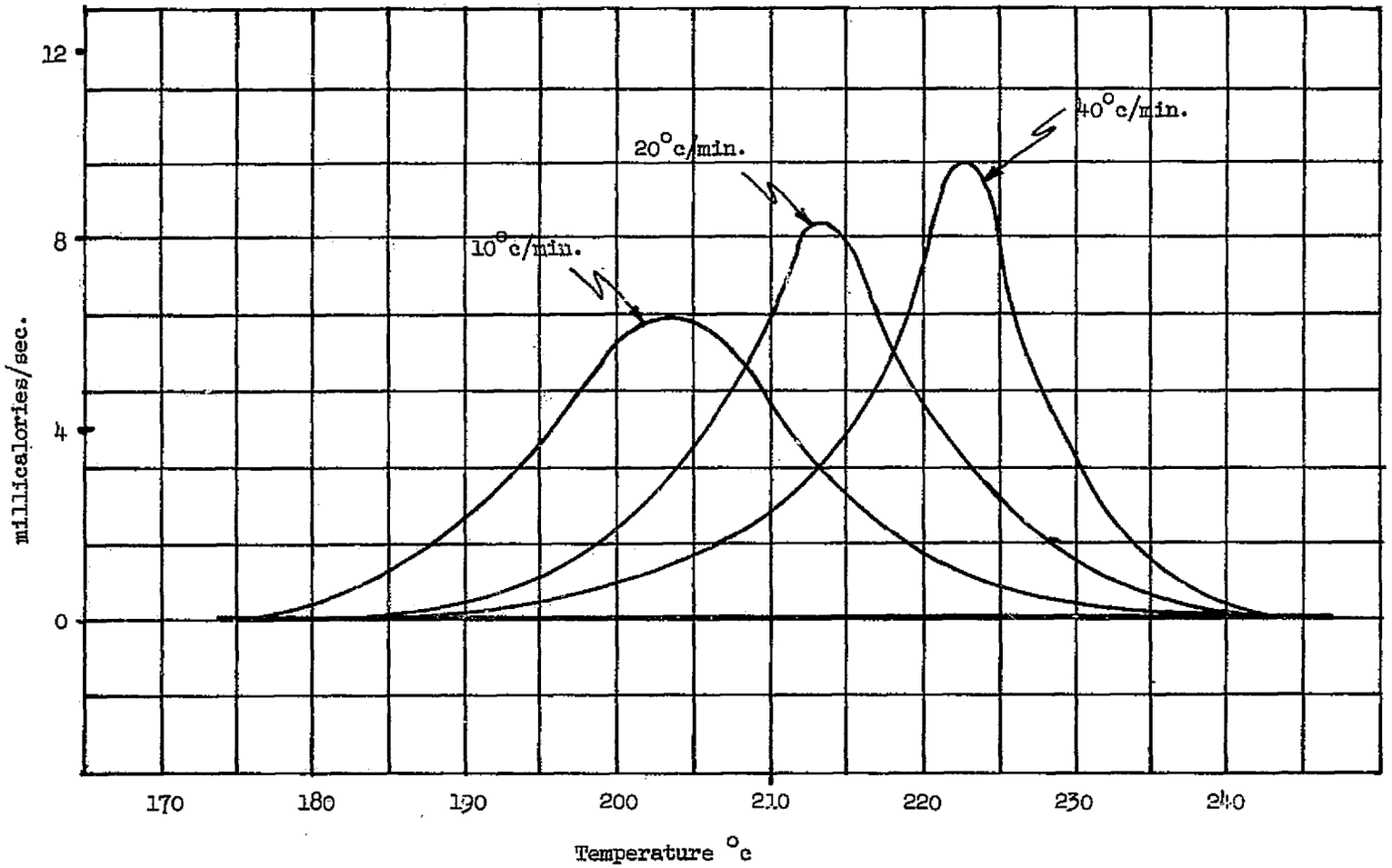

Figure 30.- Variation of curve shape for changes in scanning rate.

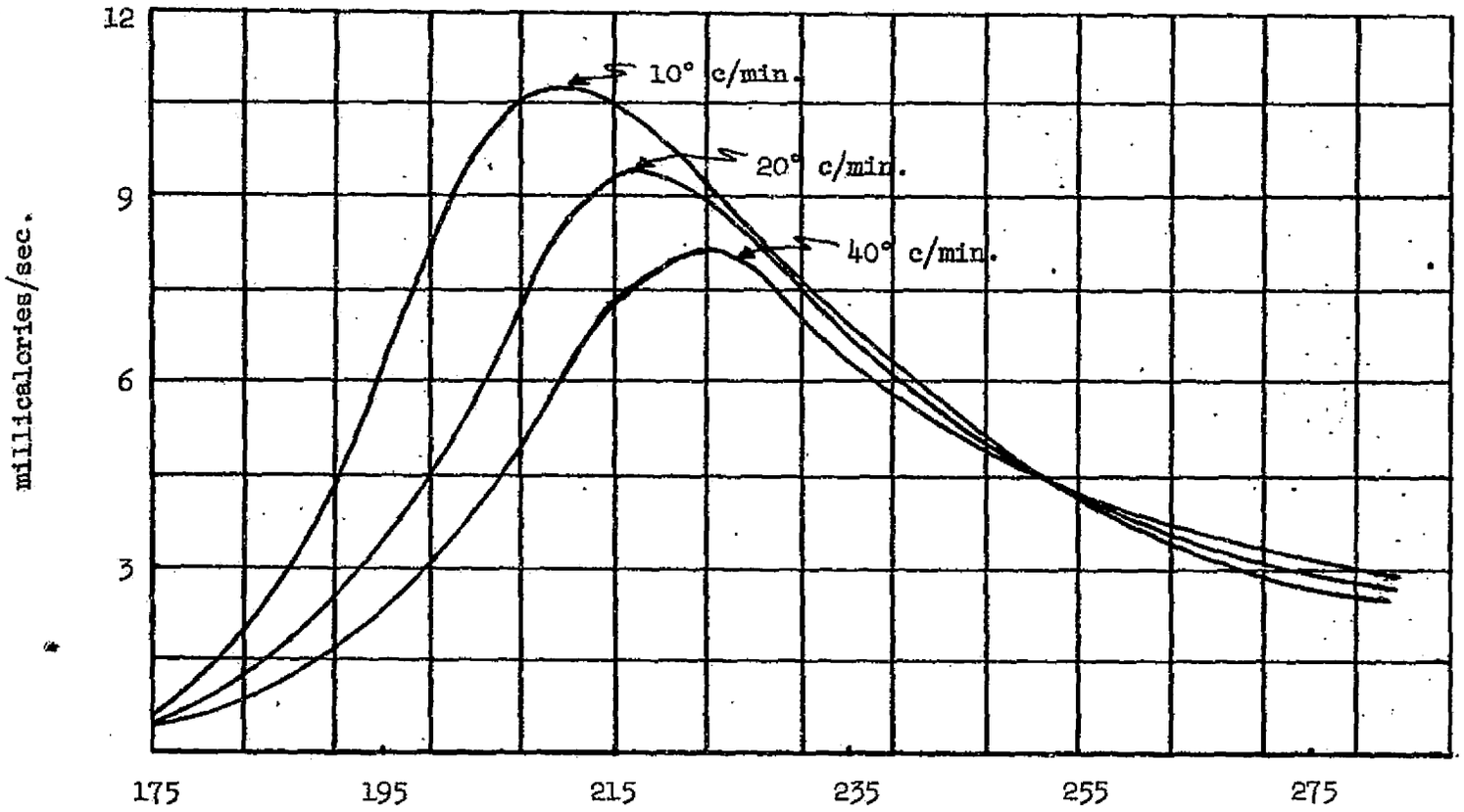

Figure 31. Computer Simulation Results

APPENDIX A

Sample Calculations

SAMPLE CALCULATIONS

1. Calculation of Activation Energy and Frequency Factor from DSC Data

First, we will derive the expression to be used. Since the rate constant is a function of temperature, it is different for each point on our curve. However, the distance from the baseline to the heat of reaction curve (fig. 17) is proportional to the rate of heat evolution. It is therefore proportional to the rate constant, provided the Arrhenius plot is a straight line. If the values of the rate constant at T_1 and T_2 are k_1 and k_2, we may write from equation (13) of the Arrhenius Theory section that

$$\ln k_1 = - \frac{E}{RT_1} + \text{constant} \qquad \text{(A-1)}$$

and

$$\ln k_2 = - \frac{E}{RT_2} + \text{constant} \qquad \text{(A-2)}$$

Subtracting (A-1) from (A-2) using $\ln(x) - \ln(y) = \ln \frac{x}{y}$, we obtain

$$\ln \frac{k_1}{k_2} = - \frac{E}{R}\left[\frac{1}{T_1} - \frac{1}{T_2}\right] \qquad \text{(A-3)}$$

and since the distances d_1 and d_2 at T_1 and T_2 are proportional to the rate constants

$$\ln \frac{d_1}{d_2} = - \frac{E}{R}\left[\frac{1}{T_1} - \frac{1}{T_2}\right] \qquad \text{(A-4)}$$

and solving for E

$$-E = R \frac{\ln d_1 - \ln d_2}{\left[\frac{1}{T_1} - \frac{1}{T_2}\right]} \qquad \text{(A-5)}$$

Beginning at the point where the heat of reaction curve deviates from the baseline, make a plot of log d versus 1/T. Use the extreme points of the straight line portion of this curve to substitute in (A-5). An example plot is given in figure 29 for the 50 mm Hg curve of figure 17. Then, using the values $\ln d_1 = 0.694$, $1/T_1 = 0.002154$, and $\ln d_2 = 3.18$, $1/T_2 = 0.002050$

$$-E = 1.986 \frac{(3.18 - 0.694)}{(0.002154 - 0.002050)} \approx 47{,}000 \frac{\text{cal}}{\text{mol}} \qquad \text{(A-6)}$$

The straight line portion of the curve usually extends from the first recognizable deviation to the point near the top of the bell-shaped curve where the inflection of the curve begins to bend over the top of the peak. This procedure was repeated for several curves at each pressure to produce the data of table I.

Notice that the calculation of the activation energy is independent of mass. If we know the mass of propellant which produced a given curve, we can calculate a frequency factor for the Arrhenius expression as follows: The distance from the baseline to the heat of reaction curve of figure 17 is the heating rate in millicalories per second produced by the mass of propellant present at that instant. Select a temperature along the bell-shaped portion of the curve which falls on the straight line portion of the Arrhenius plot as in

figure 29. At this temperature the heating rate in millicalories per second is given by

$$\dot{q} = m_T H_r f \exp\left(-\frac{E}{RT}\right) \qquad \text{(A-7)}$$

where m_T is the mass of propellant at the selected temperature T. The fraction of the sample decomposed at temperature T is A_T/A_{total} and we can write

$$m_T = \frac{A_T}{A_{total}} m_o \qquad \text{(A-8)}$$

where

m_o = initial amount of mass

A_T = area under the heat of reaction curve up to temperature T

A_{total} = total area under heat of reaction curve

The frequency factor is then given by

$$f = \frac{\dot{q}}{m_o \frac{A_T}{A_{total}} H_r \exp\left(-\frac{E}{RT}\right)} \qquad \text{(A-9)}$$

Using as an example the atmospheric pressure curve of figure 17 at T = 210° C (483° K), we have

$$m_o = 1 \text{ mg}$$

$$\frac{A_T}{A_{total}} = \frac{1}{3}$$

$$H_r = 440 \frac{\text{cal}}{\text{gm}} \text{ or } \frac{\text{millical}}{\text{mg}}$$

$$E = 51{,}500 \frac{cal}{mol}$$

$$\dot{q} = 6.3 \frac{millical}{sec}$$

Substituting these values in equation (A-9) gives

$$f = \frac{6.3}{(.10)\left(\frac{1}{3}\right)(440)\exp\left(\frac{-51{,}500}{[1.986][483]}\right)} = 4.3 \times 10^{21} \qquad \text{(A-10)}$$

2. Order of Reaction by Manual Procedure

Kuang-Hua[23] points out that in isothermal-type thermogravimetric analyses the compound under test may decompose before the desired experimental temperature is reached. This would produce unreliable results. The continuously increasing temperature method can avoid such a shortcoming. He provides an equation to calculate the rate parameters for irreversible reactions with continuously increasing temperature as follows: Let B be a volatile component in an irreversible reaction

$$aA \rightarrow bB + cC$$

The rate of weight loss for reactant A may be written as

$$-\frac{dX}{dt} = kX^n \qquad \text{(A-11)}$$

where

X = mole fraction of reactant A

k = reaction rate

n = order of reaction

Since

$$k = A \exp\left(-\frac{E}{RT}\right) \tag{A-12}$$

$$A \exp\left(-\frac{E}{RT}\right) = -\frac{\frac{dX}{dt}}{X^n} \tag{A-13}$$

Differentiating the logarithm of equation (A-13), we obtain

$$\frac{E dt}{RT^2} = d \ln\left(-\frac{dX}{dt}\right) - n \, d \ln X \tag{A-14}$$

Integrating equation (A-14) gives

$$-\frac{E}{R} \Delta \frac{1}{T} = \Delta \ln\left(-\frac{dX}{dt}\right) - n \Delta \ln X \tag{A-15}$$

Dividing equation (A-10) by $d \ln X$ and equation (A-11) by $\Delta \ln X$, we get

$$\frac{R dt}{RT^2 d \ln X} = \frac{d \ln\left(-\frac{dX}{dt}\right)}{d \ln X} - n \tag{A-16}$$

and

$$\frac{-\frac{E}{R} \Delta\left(\frac{1}{T}\right)}{\Delta \ln X} = \frac{\Delta \ln\left(-\frac{dX}{dt}\right)}{\Delta \ln X} \tag{A-17}$$

A plot of $\Delta(1/T)/\Delta \ln X$ versus $\Delta \ln(-dX/dt)/\Delta \ln X$ should produce a straight line of slope $-E/R$ and intercept n.

In order to put this into a more usable form, let M equal the total number of moles in the reaction mixture and m_a equal the moles of reactant A at time t. Then $X = m_a/M$ may be substituted in equation (A-13) and the same procedure followed to obtain

$$\ln k = \ln M^{n-1} + \ln\left(\frac{dm_a}{dt}\right) - n \ln(m_a) \qquad \text{(A-18)}$$

and

$$\frac{-\frac{E}{R}\Delta\left(\frac{1}{T}\right)}{\Delta \ln m_a} = \frac{\Delta \ln\left(-\frac{dm_a}{dt}\right)}{\Delta \ln m_a} - n \qquad \text{(A-19)}$$

The weight or volume of the reactant may be measured to replace M and m_a using

$$-\frac{dm_a}{dt} = -\frac{m_o}{w_c}\frac{dw}{dt} \qquad \text{(A-20)}$$

and

$$w_r = w_c - w \qquad \text{(A-21)}$$

where

m_o = initial mole fraction of A

w_c = weight loss after reaction is completed

w = total weight loss in time t

$\frac{dw}{dt}$ = reaction rate in time t

Using equations (A-19), (A-20), and (A-21), we obtain

$$\frac{-\frac{E}{R}\Delta\left(\frac{1}{T}\right)}{\Delta \ln w_r} = \frac{\Delta \ln\left(\frac{dw}{dt}\right)}{\Delta \ln w_r} - n \qquad \text{(A-22)}$$

A straight line should be obtained when $\Delta \ln(dw/dt) / \Delta \ln w_r$ is plotted versus $\Delta(1/T) / \Delta \ln w_r$ with intercept equal to the order of reaction n and slope equal to E/R.

3. Order of Reaction Computer Program

Details are omitted for brevity. It is hoped that this discussion, following Farmer[28], and the Fortran statements will provide the reader with an overall concept of the procedure.

Assume a rate equation of the form

$$-\frac{1}{m_o}\frac{dm}{dt} = \left(\frac{m - m_r}{m_o}\right)^n A \exp\left(-\frac{E}{RT}\right) \qquad (A-23)$$

where

m = mass at time t

m_o = initial amount of mass

m_r = residual mass at completion of reaction

A = pre-exponential factor in Arrhenius equation

E = activation energy

R = gas constant

T = absolute temperature

n = order of reaction

Multiply the top and bottom of the left-hand side of equation (A-19) by $\dot{T} = dT/dt$, which is an experimentally controlled constant, to obtain

$$-\frac{\dot{T}}{m_o}\frac{dm}{dT} = \left(\frac{m - m_r}{m_o}\right)^n A \exp\left(-\frac{E}{RT}\right) \qquad (A-24)$$

If as $\dot{T} \to 0$, $dm/dt \to 0$, then $m_{T=0} = m_o$. Integrating (A-24) gives

$$-\frac{1}{m_o}\int_{m_o}^{m}\left(\frac{m - m_r}{m_o}\right)^{-n} dm = \frac{A}{\dot{T}}\int_o^T \exp\left(-\frac{E}{RT}\right)dT = K \qquad (A-25)$$

Performing the integration of the left side

$$K = -\ln\left(\frac{m - v}{m_o}\right); \quad n = 1 \tag{A-26}$$

and

$$K = (n - 1)^{-1}\left[\left(\frac{m - m_r}{m_o}\right)^{1-n} - \left(1 - \frac{m_r}{m_o}\right)^{1-n}\right] \quad \text{for} \quad n \neq 1 \tag{A-27}$$

The right-hand integral of (A-25) may be expressed as

$$K = \frac{AE}{RT} P(X) \tag{A-28}$$

where

$$P(X) = \frac{e^{-X}}{X} - \left[-E_i(X)\right] \tag{A-29}$$

and

$$X = \frac{E}{RT}$$

The term $\left[-E_i(-X)\right]$ is the exponential integral. $-E_i(-X)$ can be approximated by[26]

$$-E_i(X) = X^{-1} e^{-X}\left(\frac{X^2 + a_1X + a_2}{X^2 + b_1X + b_2}\right) \tag{A-30}$$

where

$a_1 = 2.334733$ $\quad$ [illegible] $= 3.330657$

$a_2 = 0.250621$ $\quad$ $b_2 = 1.681534$

Therefore,

$$\left.\begin{array}{l} -\ln\left(\dfrac{m - m_r}{m_o - m_r}\right) \quad \text{for} \quad n = 1 \\ (n-1)^{-1}\left[\left(\dfrac{m - m_r}{m_o}\right)^{1-n} - \left(1 - \dfrac{m_r}{m_o}\right)^{1-n}\right] \quad \text{for} \quad n \neq 1 \end{array}\right\} = \frac{AE}{R\dot{T}} P(X) = K \tag{A-31}$$

The computer program uses equation (A-31) in an iteration scheme to find the parameters in the following sequence. The masses and temperatures at points from the experimental curve and a range of trial orders are the inputs to the program.

Step 1. Select the first trial value of n.

Step 2. Assume a trial value for E of 10,000.

Step 3. At the beginning temperature T_1 of the selected interval

$$K_1 = \frac{A_1 E}{\dot{T}R} P(X)_1 \text{ or } A_1 = \frac{\dot{T}RK_1}{EP(X)_1} \tag{A-32}$$

and at T_2

$$K_2 = \frac{A_2 E}{\dot{T}R} P(X)_2 \text{ or } A_2 = \frac{\dot{T}RK_2}{EP(X)_2} \tag{A-33}$$

For this value of n and the starting value of E, A_1 and A_2 are computed.

Step 4. The program then iterates to find a value of E which will make $A_1 = A_2$; that is, since $A_1 = A_2$

$$\frac{\dot{T}RK_1}{EP(X)_1} = \frac{\dot{T}RK_2}{EP(X)_2} \tag{A-34}$$

from which

$$\frac{K_1}{K_2} = \frac{P(X)_1}{P(X)_2} \tag{A-35}$$

The program balances this equation, using different E's in

$$X_1 = \frac{E}{RT_1} \quad \text{and} \quad X_2 = \frac{E}{RT_2} \tag{A-36}$$

Step 5. These values of A and E are recorded for the assumed value of n which is held constant for each cycle.

Step 6. Then, using the input mass values, compute (m/m_o) for the entire curve.

Step 7. Using these values, compute the errors

$$\epsilon_1 = \sum_{i=1}^{y} \left[\left(\frac{m}{m_o}\right)_{calc} - \left(\frac{m}{m_o}\right)_{exp} \right]_i \tag{A-37}$$

$$\epsilon_2 = \sqrt{\frac{\sum_{i=1}^{y} \left[\left(\frac{m}{m_o}\right)_{calc} - \left(\frac{m}{m_o}\right)_{exp} \right]_i^2}{y}} \tag{A-38}$$

where y = number of input data points. These are computed for n = 1

$$\left(\frac{m}{m_o}\right) = \frac{m_r}{m_o} + \left(\frac{m_o - m_r}{m_o}\right) \exp\left(- \frac{AT^2}{\dot{T}\frac{E}{R}} e^{-E/RT} \right) \tag{A-39}$$

and for $n \neq 1$

$$\left(\frac{m}{m_o}\right) = \frac{m_r}{m_o} + \left[\left(\frac{m_o - m_r}{m_o}\right)^{1-n} + \frac{(n-1)AT^2}{\dot{T}\frac{E}{R}} \exp\left(-\frac{E}{RT}\right)\right]^{1/1-n} \qquad \text{(A-40)}$$

Step 8. At this time, we have a set of errors for each trial value of n of the form

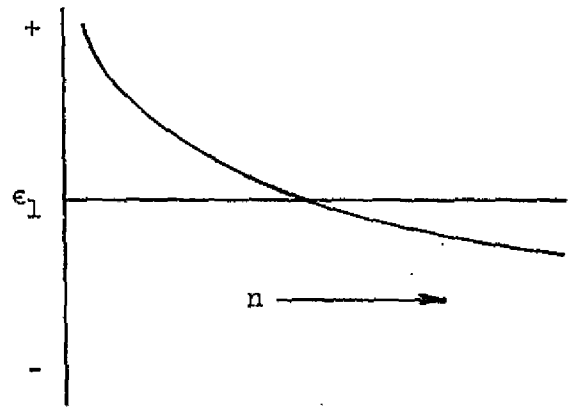

A linear fit is applied to the curve in the vicinity of where ϵ_1 changes sign and this value of n where $\epsilon_1 = 0$ is found. This is n_{min}. This and the recomputed values of A and E are printed in the last row of each series of trial values of n as the calculated best fit.

A discussion of the errors involved in using the first term in the series approximation of the exponential integral is given by Nelson[27]. A listing of the Fortran statements for this program is given in appendix B.

4. Computer Program for DSC Simulation

The bell-shaped curves of figure 17 result from two effects. First, heat is produced as a function of temperature at some exponential rate described by an Arrhenius expression. This can be described by a curve as follows:

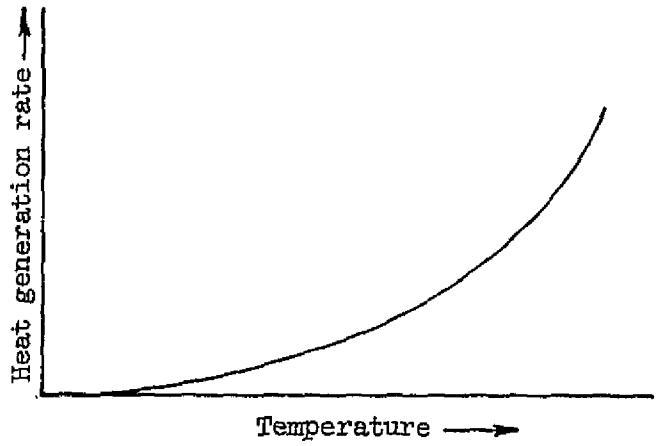

As this reaction proceeds, the mass of the original sample decreases as follows:

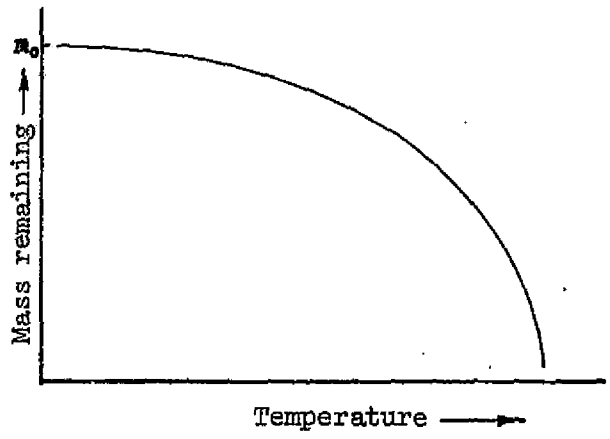

Even though the heating rate per unit mass continues to increase with temperature, a point is eventually reached at which the mass remaining is so small that the combined effect begins to decrease and returns toward zero when the reacting mass approaches zero. The combination of these two curves produces the bell-shaped curves of fi . 17. The area under this curve is the total heat produced in the reaction. The heat release effect is described by

$$H_r f \exp\left(-\frac{E}{RT}\right)$$

where

H_r = total heat of reaction, cal/gm

f = frequency factor for heat release rate

E = activation energy for heat release rate

R = gas constant

T = temperature

All parameters in this expression are known from DSC measurements. The remaining portion of our desired expression must describe the mass loss rate, and it is obtained as follows: We have already measured the mass loss rate with the TGA system and evaluated it with the computer program described in the previous section. This program provides us with a means of expressing mass as a function of time of the proper order for our particular sample and heating rate range. Using the same assumed form of the rate equation (i.e., eq. (A-23), follow the steps described in going to equation (A-28). By using an asymptotic expansion for $-E_i(-X)$, equation (A-29) can be written as

$$K = \frac{AE}{R\dot{T}}\left(1 - \frac{2!}{X} + \frac{3!}{X^2} - \frac{4!}{X^3} + \ldots\right)X^{-2}\, e^{-X} \qquad \text{(A-41)}$$

If the first term of the series is defined as

$$q(X) = X^{-2}\, e^{-X} \qquad \text{(A-42)}$$

then K may be expressed as

$$K = r\,\frac{AE}{R\dot{T}}\,q(X) \qquad \text{(A-43)}$$

where

$$r = \frac{P(X)}{q(X)} \qquad \text{(A-44)}$$

The term (1 - r) is the relative error associated with using only the first term of the series. Nelson[27] provides a plot of (1 - r) as a function of X which indicates that for X greater than 20, r is a slowly varying function approaching the value 1.0. Combining equations (A-42) and (A-43) gives

$$K = rT^2 \frac{AR}{E\dot{T}} \exp\left(-\frac{E}{RT}\right) \qquad \text{(A-45)}$$

Evaluating equation (A-27) for our particular case with an apparent second-order process and taking $m_r = 0$, we get

$$K = \left(\frac{m_o}{m} - 1\right) \qquad \text{(A-46)}$$

Setting this equal to equation (A-45) with $r = 1$ and solving for m, we obtain

$$m = \frac{m_o}{1 + T^2 \frac{AR}{E\dot{T}} \exp\left(-\frac{E}{RT}\right)} \qquad \text{(A-47)}$$

Combining this with our heat release expression and integrating with respect to time gives

$$Q(\tau) = \int_o^\tau \frac{m_o}{1 + T^2 \frac{AR}{E\dot{T}_o} \exp\left(-\frac{Ed}{RT}\right)} H_r f \exp\left(-\frac{E}{RT}\right) d\tau \qquad \text{(A-48)}$$

where

τ = time in minutes

$Q(\tau)$ = the heat of the reaction at time τ

m_o = initial mass of sample

$\dot{T}_o$ = temperature scan rate, ^oC/min

Ed = activation energy for mass loss rate

This equation is solved on the digital computer by rewriting it as

$$0 = \int_o^{\tau} \frac{m_o}{1 + \left[T_i + \dot{T}_o\tau\right]^2 \frac{AR}{E\dot{T}_o} \exp\left(\frac{-Ed}{R\left[T_i + \dot{T}_o\tau\right]}\right)} H_r f \exp\left(\frac{-E}{R\left[T_i + \dot{T}_o\tau\right]}\right) d\tau - Q(\tau) \qquad \text{(A-49)}$$

where T has been replaced by $T_i + \dot{T}_o\tau$. The integral is evaluated for different values of Ed between 20,000 and 60,000 cal/mole, using the TRAP subroutine shown as the last page in appendix B. The same iteration subroutine as used in the order of reaction program (i.e., ITR-2) is then used to find which value of Ed in this range makes the equation equal zero. Ed is first found for a heating rate of $\dot{T}_o = 20^oC$ per minute. Using this value of Ed, the integral curve is plotted. This is considered as the reference curve. This same value of Ed is used again for $\dot{T}_o = 10^o$ and 40^o C per minute. These curves are plotted and compared to the reference curve. The resulting plots are shown in figure 31.

The values used for the sample case are based on 1.0 mg of propellant at atmospheric pressure. These values are:

$M_o = 0.001$ gm $\quad T_i = 446^o$ K $\quad \dot{T}_o = 20, 10, 40^o$ K/min $\quad A = 10^{23}$

$R = 1.986 \quad f = 10^{21} \quad E = 51{,}500$ cal/mole $\quad H_r = 439$ cal/gm

APPENDIX B

Computer Statement Lists

```
      PROGRAM ITER(INPUT,OUTPUT,TAPE5=INPUT)
      INTEGER CHANGE
      REAL M1,M2,MC,MR,K1,K2,N,NFIN,NINC,NO,M,MMOE,MMOC,NMIN
      DIMENSION T(30),M(30),MMOC(30),MMOE(30),N(25),SUM(25),G(25,1),
     1 W(25),RESID(25,1),SUB(1),ARR(3,3),B(3,1),C(25,3)
      COMMON/BLK1/SUM,NN,CHANGE,ERR,I
      COMMON/BLK2/AO,A1,EC,E1,K1,K2,TDOT,E,A,R,T1,T2,T,ICODE,M,K
      NAMELIST/NAM1/MO,MR,R,TDOT,XNO,XNFIN,XNINC,XNN,K,M,T
  101 READ(5,1)
    1 FORMAT(1H                                                          )
      PRINT 1
      READ(5,NAM1)
      PRINT 3,MO,MR,TDOT,R
    3 FORMAT(1HO,3HMC=F7.3,5X,3HMR=F7.3,5X,5HTDOT=F7.3,5X,2HR=F6.3//)
      PRINT 8
    8 FORMAT(5X,1HN,7X,2HM1,6X,2HM2,10X,1HE,17X,1HA//)
      NMIN=0.
      I=1
      NO=XNO
      NFIN=XNFIN
      NINC=XNINC
      NN=XNN
      N(I)=NC
      J=1
      INC=1
  300 T1=T(J)
      KK=J+INC
      T2=T(KK)
      M1=M(J)
      M2=M(KK)
  310 CALL CALC(N(I),M1,M2,MR,MO)
      IF(ICODE.NE.0) GO TO 400
      PRINT 5,N(I),M1,M2,E,A,SUM(I),ERR
    5 FORMAT(1X,3F8.3,4E17.8)
      GO TO 500
  400 PRINT 7,N(I),M1,M2,ICODE
    7 FORMAT(1X,3F8.2,18HNO SOLUTION,ICODE=I2)
  500 IF(N(I).GE.NFIN)GO TO 600
      I=I+1
      N(I)=N(I-1)+NINC
      GO TO 300
  600 CALL CHECK(ICH)
```

```
      IF(CHANGE.EQ.0)GO TO 200
      I=ICH
      NO=N(I-1)
      NINC=NINC/2.
      NFIN=N(I+1)
      NN=5
      I=1
      N(I)=NO
  330 CALL CALC(N(I),M1,M2,MR,MO)
      IF(ICODE.NE.0) GO TO 400
      IF(I.EQ.NN)GO TO 320
      I=I+1
      N(I)=N(I-1)+NINC
      GO TO 330
  320 DO 30 II=1,NN
      W(II)=1.
   30 G(II,1)=SUM(II)
      CALL LSQPOL(N,G,W,RESID,NN,SUB,1,ARR,B,2,C,25,3)
      NMIN=(-B(1,1))/B(2,1)
      CALL CALC(NMIN,M1,M2,MR,MO)
      PRINT 5,NMIN,M1,M2,E,A,SUM(I),ERR
  200 I=1
      PRINT 9
    9 FORMAT(1H0)
      N(I)=XNO
      NINC=XNINC
      NFIN=XNFIN
      NN=XNN
      IF(KK.EQ.K)GO TO 301
      J=J+1
      GO TO 300
  301 IF(INC.EQ.3)GO TO 101
      INC=INC+1
      J=1
      GO TO 300
      END
```

```
      SUBROUTINE CALC(N,M1,M2,MR,MO)
      REAL M1,M2,MC,MR,K1,K2,N,NFIN,NINC,NO,M,MMOE,MMOC,NMIN
      COMMON/BLK1/SLM,NN,CHANGE,ERR,I
      COMMON/BLK2/AO,A1,BO,B1,K1,K2,TDOT,E,A,R,T1,T2,T,ICODE,M,K
      DIMENSION MMOC(30),MMOE(30),T(30),M(30),SUM(25)
      EXTERNAL FOFX
      DATA AO,A1,BO,B1/.250621,2.33733,1.681534,3.330657/
      A1=2.334733
      DATA XLOW,XUP,E1,E2,MAXI,DELTX/100.,2E+09,2*.0001,100000,500./
      IF(ABS(N    -1.).LT.0.01)GO TO 10
      K1=(1./(N    -1.))*(((M1-MR)/MO)**(1.-N    )-(1.-MR/MO)**(1.-N    ))
      K2=(1./(N    -1.))*(((M2-MR)/MO)**(1.-N    )-(1.-MR/MO)**(1.-N    ))
      GO TO 20
   10 K1=-ALOG((M1-MR)/(MO-MR))
      K2=-ALOG((M2-MR)/(MC-MR))
   20 CALL ITR2 (E,XLOW,XUP,DELTX,FOFX,E1,E2,MAXI,ICODE)
      IF(ICODE.NE.2) GO TO 400
      X1=E/(R*T1)
      X2=E/(R*T2)
      IF(ABS(X2).GT.741.)PRINT 1,E,R,T2,X2,N
      IF(ABS(X2).GT.741.)STOP
    1 FORMAT(//5F16.5//)
      EI2=EXP(-X2)/X2*(AO+A1*X2+X2*X2)/(BO+B1*X2+X2*X2)
      A=(K2*R*TDOT)/(E*(EXP(-X2)/X2-EI2))
      IF(ABS(N    -1.).GT.0.01)GO TO 15
      FAC1=(MC-MR)/MC
      DO 1000 L=1,K
      FAC2=EXP((-A*T(L)*T(L)*EXP(-E/(R*T(L))))/(TDOT*E/R))
      MMOC(L)=MR/MO+FAC1*FAC2
 1000 MMOE(L)=M(L)/MO
      GO TO 25
   15 FAC1=((MO-MR)/MO)**(1.-N    )
      DO 3000 L=1,K
      FAC2=(A*T(L)*T(L)*EXP(-E/(R*T(L))))/((E/R)*TDOT)
      TEST=FAC1+(N    -1.)*FAC2
      IF(TEST.GE.0.)GO TO 900
      MMOC(L)=MR/MO
      GO TO 3000
  900 MMOC(L)=MR/MO+(FAC1+(N    -1.)*FAC2)**(1./(1.-N    ))
 3000 MMOE(L)=M(L)/MC
   25 SUM(I)=0.
      ERR=0.
      DO 2000 L=1,K
      ADD=MMOE(L)-MMOC(L)
      SQ=ADD**2
      SUM(I)=SUM(I)+ADD
 2000 ERR=ERR+SQ
      ERR=SQRT(ERR/K)
  400 RETURN
      END
```

```
      FUNCTION FOFX(X)
      REAL K2,K1
      COMMON/BLK2/AC,A1,BC,B1,K1,K2,TDOT,E,A,R,T1,T2,T,ICODE
      DIMENSION T(30)
      X1=X/(R*T1)
      X2=X/(R*T2)
      EI1=EXP(-X1)/X1*(AC+A1*X1+X1*X1)/(BC+B1*X1+X1*X1)
      EI2=EXP(-X2)/X2*(A0+A1*X2+X2*X2)/(B0+B1*X2+X2*X2)
      Z=(K2*R*TDOT)/(X*(EXP(-X2)/X2-EI2))
      FOFX=(Z*X/(R*TDOT)*(EXP(-X1)/X1-EI1))-K1
  700 RETURN
      END
```

```
      SUBROUTINE CHECK(ICH)
C
C    CHECKS FOR CHANGE OF SIGN IN SUM
C
      INTEGER CHANGE
      DIMENSION SUM(25)
      COMMON/BLK1/SUM,NN,CHANGE,ERR,I
      CHANGE=0
      IF(SUM(1).GE.0.)GO TO 1
      GO TO 2
    1 DO 10 I=2,NN
      IF(SUM(I).GE.0.)GO TO 10
      CHANGE=1
      ICH=I
      GO TO 100
   10 CONTINUE
      GO TO 100
    2 DO 20 I=2,NN
      IF(SUM(I).LT.0.)GO TO 20
      CHANGE=1
      ICH=I
      GO TO 100
   20 CONTINUE
  100 RETURN
      END
```

SUBROUTINE ITR2

LANGUAGE: FORTRAN

PURPOSE: Given F(X) = 0, to find a value for X within a given epsilon of relative error in a given interval (a,b).

USE: CALL ITR2 (X, A, B, DELTX, FOFX, E1, E2, MAXI, ICODE)

X The root.

A The lower bound on X. This value is used by ITR2 as an initial guess.

B The upper bound on X. This value is used by ITR2 as a final guess if the entire interval is scanned.

DELTX ΔX, the size of the scanning interval.

FOFX The name of a function subprogram to evaluate F(X).

E1 Relative error criterion.

E2 Absolute error criterion.

MAXI A maximum iteration count supplied by the user.

ICODE An integer supplied by ITR2 as an error code. This code should be tested by the user on return to the calling program.

ICODE = 0, normal return
ICODE = 1, maximum iterations are exceeded
ICODE = 2, DELTX = 0, or negative
ICODE = 3, a root cannot be found within the given bounds
ICODE = 4, A > B

RESTRICTIONS: Make A < B, ΔX positive. A function subprogram with a single argument X must be written by the user to evaluate F(X). The name of this subprogram, FOFX, must appear in an EXTERNAL statement of the

ITR2

calling program.

METHOD: The given function F(X) is evaluated at a given starting point, a, and at intervals of a specified ΔX thereafter, up to and including a specified end point, b. A change of sign of the function across a ΔX interval indicates a possible root in that interval. The interval is then halved successively toward F(X) = 0 until the prescribed accuracy is satisfied. The given function F(X) is evaluated once for each halving step.

If the given function is expected to have more than one root between the prescribed starting and end points, it is suggested that a sufficiently small ΔX be given such that no more than one root be present within a ΔX interval. A normal return is given upon the location of the first root from the starting point, a. Additional roots must be located by new entries into the subroutine using a new starting point, r, which is just beyond the previous root.

ACCURACY: The iteration process is continued until either of two convergence criteria are satisfied. These criteria are:

1. if $|X_i| > \epsilon_1$

$$\left|\frac{X_i - X_{i-1}}{X_i}\right| \leq \epsilon_1$$

2. if $X_i \leq \epsilon_1$

$$|X_i - X_{i-1}| \leq \epsilon_2$$

REFERENCE: T. B. Scarborough, NUMERICAL MATHEMATICAL ANALYSIS, Fourth Edition.

STORAGE: 260_8 locations

SOURCE: NASA, LRC, Terry A. Straeter

IDENTIFICATION: TRAP

PURPOSE: TRAP calculates the running integral of the curve $y = f(x)$.

RESTRICTIONS: Y and X can be input in table form or Y must be calculated at NL discrete points before entering TRAP.

The subroutine has been compiled with a variable DIMENSION statement. The following must be dimensioned in the calling program:

X(IL), Y(IL), SUM(IL).

USAGE: CALL TRAP (Y, X, NL, SUM, SUM1) where

Y = the name of the dependent variable.

X = the name of the independent variable.

NL = the number of points on the curve or in the table.

SUM = the location of a vector of order IL which contains the running integral of the curve $y = f(x)$. SUM(IL) is the total integral.

SUM1 = SUM(1): The initial value of the integrated curve.

METHOD: TRAP uses the trapezoidal rule of integration for a variable ΔX.

ORIGINATOR: Raye C. Mathis